The Plant Cell, Vol. 29: 960–983, May 2017, www.plantcell.org © 2017 ASPB.

LARGE-SCALE BIOLOGY ARTICLE

Multi-Omics of Tomato Glandular Trichomes Reveals Distinct Features of Central Carbon Metabolism Supporting High Productivity of Specialized Metabolites[OPEN]

Gerd U. Balcke,[a] Stefan Bennewitz,[a] Nick Bergau,[a] Benedikt Athmer,[a] Anja Henning,[a] Petra Majovsky,[b,1] José M. Jiménez-Gómez,[c,2] Wolfgang Hoehenwarter,[b] and Alain Tissier[a,3]

[a] Leibniz Institute of Plant Biochemistry, Department of Cell and Metabolic Biology, D-06120 Halle (Saale), Germany
[b] Leibniz Institute of Plant Biochemistry, Proteome Analytics, D-06120 Halle (Saale), Germany
[c] Max Planck Institute for Plant Breeding Research, 50829 Cologne, Germany

ORCID IDs: 0000-0002-0475-0672 (G.U.B.); 0000-0002-7669-7524 (W.H.); 0000-0002-9406-4245 (A.T.)

Glandular trichomes are metabolic cell factories with the capacity to produce large quantities of secondary metabolites. Little is known about the connection between central carbon metabolism and metabolic productivity for secondary metabolites in glandular trichomes. To address this gap in our knowledge, we performed comparative metabolomics, transcriptomics, proteomics, and ^{13}C-labeling of type VI glandular trichomes and leaves from a cultivated (*Solanum lycopersicum* LA4024) and a wild (*Solanum habrochaites* LA1777) tomato accession. Specific features of glandular trichomes that drive the formation of secondary metabolites could be identified. Tomato type VI trichomes are photosynthetic but acquire their carbon essentially from leaf sucrose. The energy and reducing power from photosynthesis are used to support the biosynthesis of secondary metabolites, while the comparatively reduced Calvin-Benson-Bassham cycle activity may be involved in recycling metabolic CO_2. Glandular trichomes cope with oxidative stress by producing high levels of polyunsaturated fatty acids, oxylipins, and glutathione. Finally, distinct mechanisms are present in glandular trichomes to increase the supply of precursors for the isoprenoid pathways. Particularly, the citrate-malate shuttle supplies cytosolic acetyl-CoA and plastidic glycolysis and malic enzyme support the formation of plastidic pyruvate. A model is proposed on how glandular trichomes achieve high metabolic productivity.

INTRODUCTION

Glandular trichomes (GTs) are specialized secretory cells that protrude from the epidermis of ~30% of all vascular plants (Fahn, 2000). The morphology of GTs is very diverse across plant species as exemplified by the peltate trichomes of the Lamiaceae, the biseriate trichomes of the Asteraceae, or the capitate trichomes of the Solanaceae. However, they are all multicellular and share a basic plan with basal, stalk, and one to a few (typically four to eight) glandular head cells (Croteau et al., 2005; Glas et al., 2012). The glandular head cells have in common the capacity to produce substances of relevance to the chemical communication of the plant with its environment, including short branched-chain acyl sugars, flavonoids, phenolics, alkaloids, and isoprenoids (Schilmiller et al., 2009, 2010; Schmidt et al., 2011; Kim et al., 2012; Brückner et al., 2014; Li et al., 2014). Some of these secondary metabolites were shown to have antifeedant, oviposition deterrent, and in some cases toxic properties toward insects (Coates et al., 1988; Nonomura et al., 2009; Bleeker et al., 2011, 2012; Glas et al., 2012). Furthermore, secondary metabolites produced in GTs have high commercial value in the cosmetics, food, and pharmaceutical industries. For instance, artemisinin, a sesquiterpene lactone of *Artemisia annua*, and its derivatives in combination therapy are currently regarded as the most effective treatment against malaria (Kokwaro, 2009).

One notable feature of GTs is their metabolic productivity. For example, acyl sugars (ASs) in *Solanum pennellii* can represent up to 20% of the leaf dry weight (Fobes et al., 1985), and in certain *Solanum habrochaites* accessions, sesquiterpene carboxylic acids may reach more than 12% of the leaf dry weight (Frelichowski and Juvik, 2005). These figures support the notion that GTs can be considered as highly active metabolic cell factories because the compounds are produced exclusively there. For volatile compounds, this high productivity is often associated with dedicated storage features in the GT. For example, in tomato and many Lamiaceae species, the secreted metabolites are stored in an extracellular cavity whose volume can swell to a multiple of the volume of the glandular head cells (Turner et al., 2000; Bergau et al., 2015).

To date, there is no conceptual model to explain how GTs achieve such remarkable metabolic productivity. Most studies on GT so far have focused on the identification and characterization

[1] Current address: Celerion Switzerland, Allmendstrasse 32, 8320 Fehraltorf, Switzerland.
[2] Current address: Institut Jean-Pierre Bourgin, INRA, AgroParisTech, CNRS, Université Paris-Saclay, RD10, 78026 Versailles Cedex, France.
[3] Address correspondence to alain.tissier@ipb-halle.de.
The author responsible for distribution of materials integral to the findings presented in this article in accordance with the policy described in the Instructions for Authors (www.plantcell.org) is: Alain Tissier (alain.tissier@ipb-halle.de).
[OPEN]Articles can be viewed without a subscription.
www.plantcell.org/cgi/doi/10.1105/tpc.17.00060

of enzymes directly involved in the formation of the major trichome secondary metabolites (Croteau et al., 2005; Slocombe et al., 2008; Sallaud et al., 2009; Schmidt et al., 2011; Kim et al., 2012; Schilmiller et al., 2012; Brückner et al., 2014), and no comprehensive study has been conducted to link the downstream biosynthesis steps to central and energy metabolisms in these cells. Understanding how the core metabolic network in these specialized cells is organized to deliver such high productivity levels will offer new opportunities in the breeding of plants with increased resistance to various aggressors and in metabolic engineering in general. Tomato, due to its excellent genetic resources and extensive sequence data, including sequenced genomes from cultivated tomato and several closely related wild relatives, can serve as a good model for the study of the physiology and development of GTs (Tissier, 2012). For this study, the cultivated tomato *Solanum lycopersicum* LA4024 (hereafter referred to as LA4024) and an accession from a wild relative, *S. habrochaites* LA1777 (hereafter referred to as LA1777), were chosen as study material. The most abundant GTs in both species are of type VI, which confer a distinct secondary metabolite profile to each species (Bergau et al., 2015). In LA4024, the major metabolites produced are the flavonoid rutin and various monoterpenes (e.g., α-phellandrene), whereas LA1777 produces mostly sesquiterpene carboxylic acids and acyl sugars (McDowell et al., 2011; Glas et al., 2012). Our rationale was to compare the trichomes and the respective trichome-free leaf in order to identify which features distinguish these two tissues and to understand what makes the trichomes unique. Our comparison is based on four sets of data from transcriptomics, proteomics, metabolomics, and ^{13}C-labeling, which were processed by uni- and multivariate analyses and used to address two major questions: How do GTs generate the energy needed to produce these large amounts of secondary products and what are the carbon sources that fuel metabolite production?

RESULTS

Morphology

In tomato, seven classes of trichomes have been described. Four of them are glandular, among which types I, IV, VI, and VII are present in LA1777, while types I, VI, and VII occur in LA4024 (McDowell et al., 2011; Glas et al., 2012). LA1777 is a wild tomato accession with round-shaped type VI trichomes as the dominant trichome type covering the leaf surface at high density (Figure 1). The cultivated tomato LA4024 is closely related to *S. lycopersicum* cv Heinz whose genome was recently published (Tomato Genome Consortium, 2012). Its dominating trichome type is a four-leaf clover-shaped type VI, which occurs at a lower density than in LA1777 (Bergau et al., 2015).

In both species, based on microscopy analysis, leaf trichome preparations contained ~80% type VI glandular head cells and 20% type I/IV head cells in LA1777 and 20% type I head cells in LA4024, respectively. Furthermore, it was not possible to fully remove the stalk cells of both types of glandular heads, which accounted for 37% of all harvested cells. In type VI trichomes, four glandular head cells surround a storage cavity filled with secondary metabolites, which is typically much larger in the wild tomato (Bergau et al., 2015). Like leaf mesophyll cells, the glandular head cells of type VI trichomes possess their own chloroplasts with intact thylakoid membranes, suggesting they have the capacity to generate the ATP and NADPH required for the assembly of secondary metabolites. Notably, the outer envelope (cell wall + cuticle) of type VI GT cells of both tomato species is slightly thicker than that of leaf epidermal cells (~0.7 μm versus 0.5 μm) and 3 to 5 times thicker than the double cell wall between leaf parenchyma cells (Figure 1). This suggests that, as in epidermal cells, gas and water exchanges with the outside are limited.

Metabolomics

Central metabolites are mostly polar. Therefore, to better understand the connection between primary and secondary metabolism in glandular trichomes, nontargeted profiling for polar and semipolar metabolites was performed separately using two liquid chromatography-mass spectrometry (LC-MS) methods and one gas chromatography-mass spectrometry (GC-MS) method (see Methods). Unless indicated, all metabolomics data discussed below showed significant fold changes based on pairwise *t* testing at a significance level of $P < 0.05$. For details, see Supplemental Data Sets 1 to 3.

The Trichomes of Wild and Cultivated Tomato Produce Different Secondary Metabolites

As expected, metabolite profiling of secondary metabolites revealed significant differences not only between both species but also between the trichome and leaf within a species (Figure 2; Supplemental Data Set 1). Venn diagrams show only 27% of the upregulated and 23% of the downregulated mass features in trichomes versus leaves as shared patterns between both tomato species (Supplemental Figure 1). Principal component analysis (PCA) of semipolar secondary metabolites measured by LC-MS separated both tomato lines on PC1 with 78% coverage of variance, indicating very different composition in the secondary metabolites of both species (Figure 2A). PC2 (15%) separated trichomes from leaves across the two lines, demonstrating also joined latent similarities in the patterns of leaves and trichomes, respectively. Here, signals relating to the glycoalkaloids tomatine and dehydrotomatine, which are exclusively found in the leaves, strongly contributed to the group separation. In trichomes, the total ion chromatograms of LA4024 were dominated by monoterpenes (GC-MS) and conjugated flavonols (mainly rutin; LC-MS), while sesquiterpenes (GC-MS), short branched-chain (C2-C12) acyl sugars, and sesquiterpene carboxylic acids are prevalent in LC-MS-based chromatograms of LA1777 (Supplemental Figure 2). These results confirm previous metabolite analyses of tomato trichomes and underline that trichomes of these species produce different terpenoid secondary metabolites (Slocombe et al., 2008; Besser et al., 2009; Schilmiller et al., 2010; McDowell et al., 2011; Ekanayaka et al., 2014; Ghosh et al., 2014; Li et al., 2014). When quantified, rutin alone contributed to 25% ± 3% of the corresponding trichome dry weight in LA4024, whereas the sum of two major sesquiterpene carboxylic acids [(+)-(*E*)-α-santalene-12-oic acid and (+)-(*E*)-endo-bergamotene-12-oic acid] added up to 23% ± 2% of the GT dry weight in LA1777. Both values illustrate the

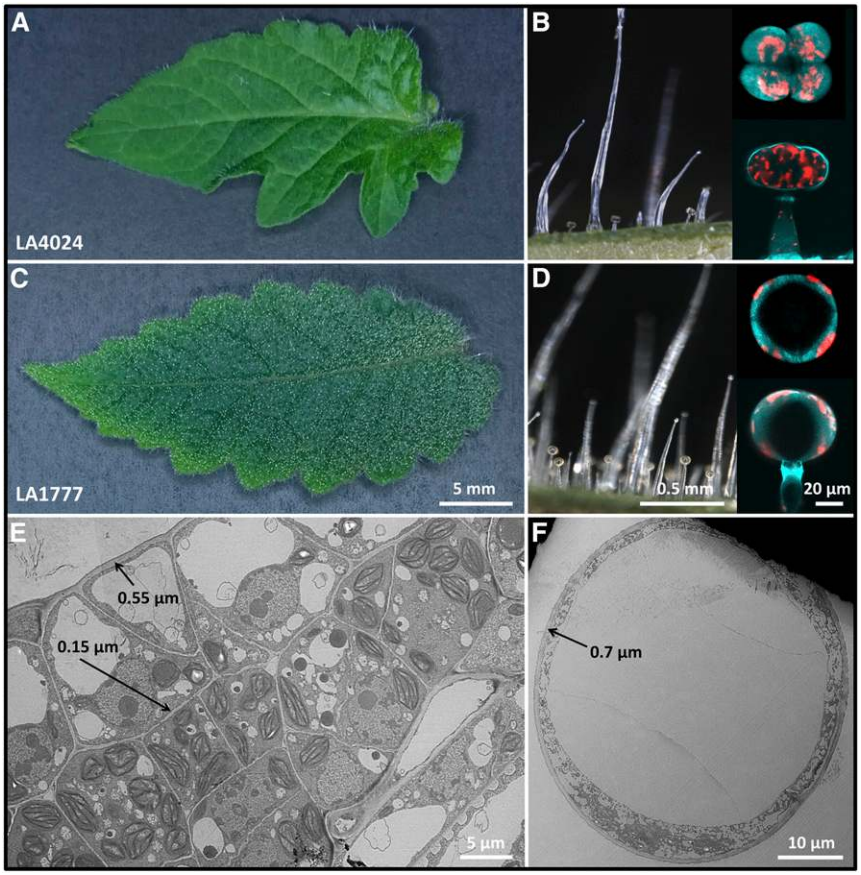

Figure 1. Bright-Field, Fluorescence, and Electron Microscopy of Type VI Glandular Trichomes.

(A) and **(C)** Light microscopy: leaflets of LA4024 **(A)** and wild-type LA1777 **(C)** showing different trichome density.
(B) and **(D)** Left side: section of leaves from LA4024 **(B)** and LA1777 **(D)** showing the epidermis and mesophyll cells; right side: fluorescence microscopy of trichome head cells from LA4024 **(B)** and LA1777 **(D)** viewed from above (top) or from the side (bottom).
(E) and **(F)** Transmission electron microscopy: section of a leaf from LA1777 highlighting the thickness of the outer cell wall and cuticle of the epidermal cells and the cell wall of internal cells **(E)**; head of a type VI trichome from LA1777 illustrating the size of the intercellular storage cavity and the thickness of the outer cell wall **(F)**.

capability of GT to direct massive carbon fluxes toward distinct classes of secondary metabolites. To estimate the productivity of type VI trichomes in the two species regarding terpenoids, we quantified the major sesquiterpene carboxylic acids, i.e., santalenoic and bergamotenoic acids, in LA1777 and the major terpenes (mostly monoterpenes and minor sesquiterpenes) in LA4024 in surface extracts of young leaflets and in parallel estimated the trichome numbers of leaflets of comparable size. We found 6563 ± 618 ($n = 3$) type VI trichomes per leaflet in LA1777 and 1804 ± 276 ($n = 5$) in LA4024. This gave 65.82 ± 7.85 ng ($n = 3$) of sesquiterpene carboxylic acids per trichome in LA1777 versus 0.68 ± 0.20 ng ($n = 5$) of terpenes per trichome in LA4024. Thus, the terpene productivity in type VI trichomes of LA1777 is around 97 times higher than in those of LA4024.

Newly Identified Metabolites Include Abundant Oxylipins Derived from C18- and C20-PUFAs

Interestingly, we detected high intensities of free saturated, monounsaturated, and polyunsaturated fatty acids (PUFAs) that were found to be preferentially enriched in the trichomes of both tomatoes (Supplemental Figure 3A). The most abundant were 18:2 linoleic and 18:3 linolenic acid in both species and a C20:3-eicosatrienoic and C20:4-arachidonic acid in LA1777. The presence of polyunsaturated C20 fatty acids in LA1777 is noteworthy, since these are rare in plants and were shown to modulate plant responses to stress (Savchenko et al., 2010). Corresponding to the chain length of the fatty acids, numerous oxylipins that strongly accumulated in GTs compared with the corresponding leaves were also detected. Among these, dihydroxy-C18:1/C18:2, hydroxy-C18:2/C18:3, trihydroxy-C18:3, hydroxy-C20:2/C20:3/C20:4, and dihydroxy-20:4/C20:5 were most abundant, with the C20-oxylipins again accumulating preferentially in LA1777 (Supplemental Figure 3B). We compared LC retention time and the MS^2 spectra of hydroxy-C18:2 with authentic standards of the oxylipins 13*S*-hydroxy-9*Z*,11*E*-octadecadienoic acid [13(*S*)-HODE] and 9*S*-hydroxy-10*E*,12*Z*-octadecadienoic acid [9(*S*)-HODE]. Both substances with a precursor ion [M-H] of 295.227 atomic mass units coeluted with a peak at 13.6 min, which was

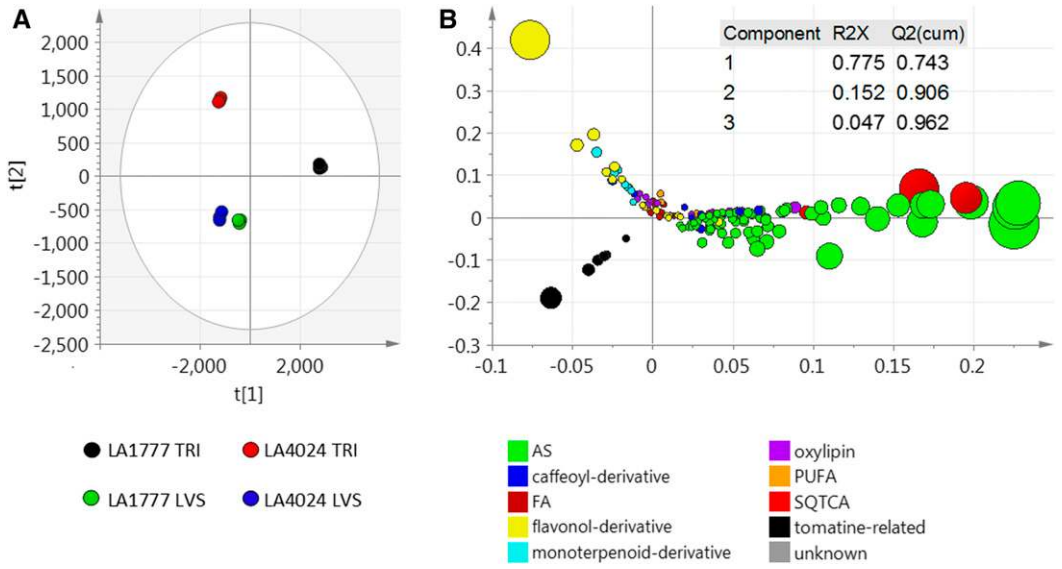

Figure 2. Principle Component Analysis of Semipolar Metabolites Measured in Negative ESI Mode.

The data consist of 3476 signals, each corresponding to a unique *m/z* and retention time combination. Scores **(A)** and loadings **(B)**. In the loading plot, the colors of the circles correspond to metabolite classes of interest, and the size of the circle reflects the average pool size of the respective metabolite over all of the samples. For simplicity, only signals that could be associated with a metabolite group are shown (in total 129). The entire data set, i.e., including unknowns, is presented in Supplemental Data Set 1. All data are weight-normalized and Pareto-scaled. FA, fatty acids; SQTCA, sesquiterpene carboxylic acid; R2X, cumulative sum of squares of the entire X explained by principal components 1 to 3. X = log-normalized peak heights relative to LA1777 leaf matter; Q2X(cum) = cumulative fraction of the total variation of X and Y that can be predicted by principal components.

also observed in GTs of both species. Yet, collision-induced dissociation (CID) spectra of the compound from LA1777 trichomes matched the CID spectra of 9(*S*)-HODE, whereas those from LA4024 trichomes matched the spectra of 13(*S*)-HODE (Supplemental Figure 4).

Trichome-Specific Features of Central Carbon and Energy Metabolism

To survey the hydrophilic metabolites involved in central carbon and energy metabolism, we compared the peak areas of 115 selected MS^1 mass/retention time features of known identity. Those included intermediates of the tricarboxylic acid (TCA) cycle, sugar phosphates, free amino acids, redox couples of glutathione and NAD cofactors, as well as nucleotides and intermediates of both isoprenoid precursor pathways. Venn analysis showed that more than one-third of all signals were shared across both tomato models as common features between trichomes and leaves, respectively (Supplemental Figure 1).

PCA identified three principal components which cover 89.4% of the variance in the data. In this case, PCA showed a stronger group separation between trichomes and leaves across the tomato lines (PC1 37.9%) than the separation between both tomato lines on PC2 (33.8%). This indicates that, regardless of the tomato species, type VI GTs have a highly distinct central carbon and energy metabolism compared with leaves (Supplemental Figure 5). Also, cross-validation using five out of six series per tomato species to predict the missing data series and a good predictability of metabolome data of LA4024 from LA1777 and vice versa underline this (Supplemental Data Set 4). To identify features that distinguish trichomes from leaves as the response variables, partial least square (PLS) analysis was performed individually for both species. This analysis showed a strong group separation based on Calvin-Benson-Bassham (CBB) cycle intermediates, ADP-glucose, and glycerate with lower peak intensities in trichome samples compared with leaves (e.g., ribulose-1,5-bisphosphate, 9.2-fold [LA1777], 8.6-fold [LA4024]; 3-phosphoglycerate, 5.3-fold [LA1777], 1.7-fold [LA4024]; ADP-glucose, 10.6-fold [LA1777], 8.6-fold [LA4024]) (Figure 3; Supplemental Data Set 3). Notably, the latter metabolites are involved in photosynthetic carbon fixation and in starch biosynthesis, which appear to be less active in trichomes than in leaves. Besides this, trichomes of LA1777 and LA4024 accumulated large amounts of inositol polyphosphates (IP_5 and IP_6), which were not detected in the leaves (Supplemental Data Set 3).

Similarly, oxidized glutathione showed increased levels in the trichomes of both species (i.e., in LA1777, GSSG, 1.2-fold [P = 0.07]; in LA4024, GSSG, 1.9-fold; Supplemental Data Set 3). Although the reduced form of glutathione was 1.5-fold (LA1777) and 3.7-fold (LA4024) higher in the leaves, importantly, the ratio between oxidized and reduced glutathione is shifted to much higher values in GTs than in leaves (in LA1777, leaves, 0.9, GTs, 1.7; in LA4024, leaves, 0.4, GT, 2.8). Thus, in trichomes, a much larger fraction of the glutathione pool is oxidized. Moreover, cysteine levels were 4.6 and 5.3 times higher in GTs of LA1777 and LA4024, respectively, implying increased replenishment of GSH in GTs. Ascorbate, another electron scavenger, showed decreased levels in trichomes relative to leaves in LA1777 (2.5-fold) and was

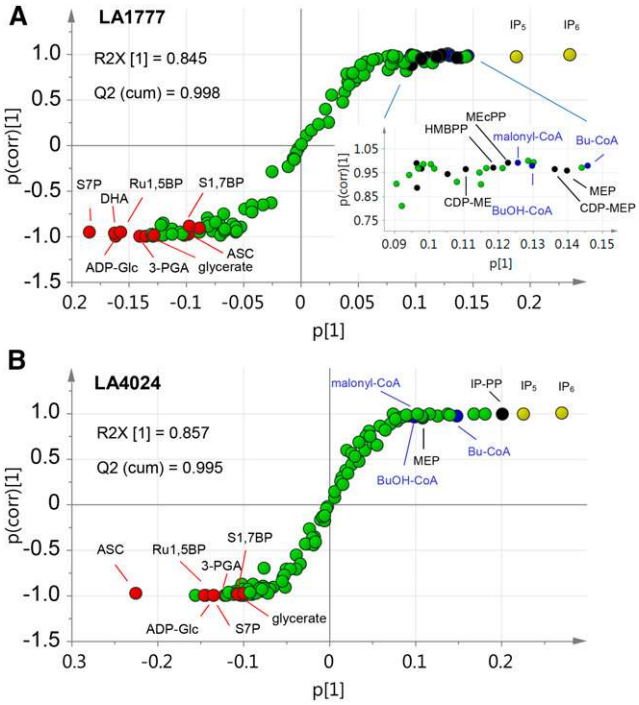

Figure 3. Loadings of PLS Analyses of 115 Selected MS Signals from Hydrophilic Extracts.

(A) Analysis of polar metabolites of LA1777.
(B) Analysis of polar metabolites of LA 4024.
Red, related to photosynthesis and starch formation; black, related to isoprenoid biosynthesis; blue, lipid; yellow, inositol polyphosphates. For abbreviations, see Supplemental Data Set 3. R2X[1]: cumulative sum of squares of the entire X explained by principal component 1. X = log-normalized peak heights relative to LA1777 leaf matter; Q2X(cum) = cumulative fraction of the total variation of X that can be predicted by principal component 1 for all of its x-variables (response variables: 1 = GT; 2 = leaves). Mutual predictability for both data sets was demonstrated in Supplemental Data Set 4.

strongly depleted in the trichomes of LA4024 (Figure 3; Supplemental Data Set 3).

TCA intermediates such as aconitate and succinate were increased in trichomes versus leaf (aconitate, 1.4-fold [LA1777], 3.5-fold [LA4024]; succinate, 2.3-fold [LA4024]) or showed no significant difference between trichome and leaf (LA1777). Finally, cyclic forms of AMP and GMP showed much higher intensities in GTs than in leaves (cAMP, 4.0-fold, cGMP, 3.5-fold [LA1777]; cAMP, 9.2-fold, cGMP, 18.4-fold [LA4024]) (Supplemental Data Set 3). Interestingly, the ATP levels in leaves and trichomes were comparable for both tomato species (Supplemental Data Set 3).

Intermediates of Secondary Metabolite Precursor Pathways Are Overrepresented in Trichomes

Since GTs of LA4024 and LA1777 in particular produce terpenoids from both the mevalonate (MEV) and the 2-*C*-methyl-D-erythritol 4-phosphate (MEP) pathways, metabolites of these pathways were measured, when possible. 3-Hydroxy-3-methylglutaryl-CoA, an intermediate of the isoprenoid biosynthesis via the MEV pathway, also showed increased levels in the trichomes of both species (2.5-fold [LA1777] and 4.3-fold [LA4024]) versus leaves (Supplemental Data Set 3). In LA1777, intermediates of the MEP pathway showed up to 7-fold higher levels in trichomes than in leaves (Supplemental Data Set 3) and are major contributors to the group separation between leaves and trichomes of both species (Figure 3A). Correspondingly, signals for cytidyl nucleotides, which are required for this pathway (Caspi et al., 2014), are significantly upregulated in the trichomes (Supplemental Data Set 3). These results are in accordance with the high levels of sesquiterpenoids that are synthesized in the plastids of GT via the MEP pathway in LA1777 (Besser et al., 2009; Sallaud et al., 2009; Schilmiller et al., 2009). By contrast, metabolic levels of the MEP pathway intermediates and cytidyl nucleotides were not or moderately increased in GTs of LA4024, with MEP showing a 3.7-fold higher level than in the corresponding leaf as the metabolite with the largest difference (Supplemental Data Set 3). Threonine and valine, which are involved in the formation of branched short-chain acyl residues of ASs, were significantly elevated in the trichomes of LA1777 but not in LA4024, where ASs were much less abundant (Supplemental Data Set 3). In agreement with the increased lipid formation in GTs of both species (see above), malonyl-CoA was strongly increased in GT (4.3-fold [LA1777] and 2.5-fold [LA4024]) (Supplemental Data Set 3).

Together, the metabolite profiles of hydrophilic metabolites reflect that intermediates required for the biosynthesis of trichome-specific secondary metabolites are present at high levels, especially for the biosynthesis of terpenoids. In addition, glandular trichomes of LA1777 appeared to be metabolically more active than those of LA4024.

Transcriptomics, Proteomics, and ^{13}C-Labeling

To correlate our metabolomics data with gene expression, we performed transcriptomic and proteomic analysis on the same samples. The transcriptomics data were generated with a custom-designed microarray based on RNA-seq data that were produced for this project (see Methods).

We report quantile-normalized transcriptome data and proteome data of biological triplicates of isolated trichomes and trichome-free leaves (Supplemental Data Set 5). Unless indicated, all data discussed below showed significant fold changes at a significance level $P < 0.05$. A global overview of the relative transcript and protein levels in trichomes and trichome-free leaves with regards to cellular metabolism is provided in Figure 4 (transcriptomics of LA1777) and Supplemental Figures 6 and 7 (transcriptomics and proteomics of LA4024 and proteomics of LA1777). Venn diagrams showing common patterns of leaf and trichome-specific -omics data across both tomato models (~26–30%) as well as species-specific data are shown in Supplemental Figure 1.

Glandular Trichomes Constitute a Strong Sucrose Sink with Low CBB Activity but High Expression of Photosystem Genes

One outstanding question concerns the origin of the carbon supply to GTs. Unlike mint (*Mentha x piperita*) peltate GTs, tomato

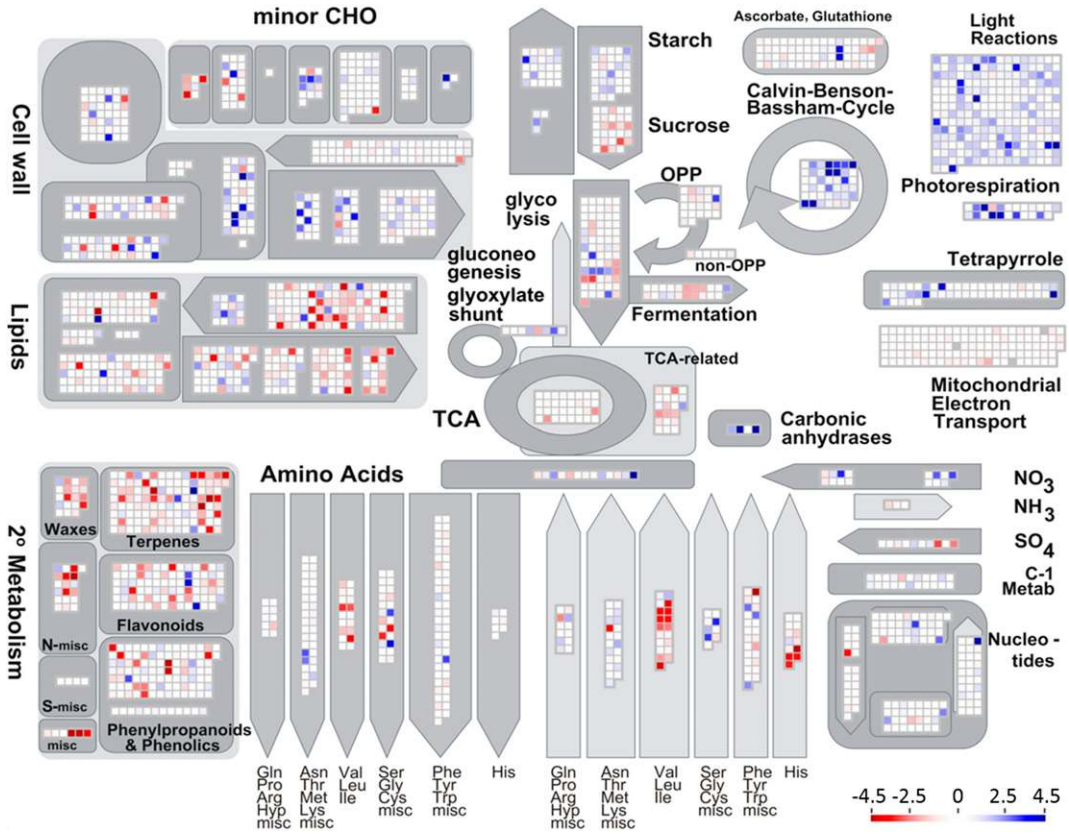

Figure 4. MapMan Overview of the Transcriptomics of Cellular Metabolism in LA1777.

The color scale (bottom right hand corner) corresponds to $\log_2$-fold changes for trichome versus trichome-free leaves with red being significantly overexpressed in trichomes and blue overexpressed in leaves ($P < 0.05$, Fisher exact *t* test). White squares: $\log_2$-fold changes between -1 and 1 or *t* test, $P > 0.05$.

GTs possess chloroplasts. This raises the question of whether carbon fixation takes place in these cells and, if so, to what extent it contributes to the carbon supply of the GTs or if they depend on leaves as their main carbon supplier. To answer these questions, we examined our transcriptomics and proteomics data. First, analysis of the transcriptome data of genes involved in sucrose degradation showed that several cell walls and cytosolic invertases as well as sucrose synthases were significantly ($P < 0.05$ with *t* test statistics) overrepresented in trichomes compared with leaves (Figure 5). This is particularly clear for sucrose synthases where the cumulative expression of the two major isoforms is 7.5 and 7.4 times higher in GTs in LA1777 and LA4024, respectively. Conversely, the cumulated expression of invertase inhibitors is 10.5- and 19.3-fold stronger in leaves versus trichomes of LA1777 and LA4024, respectively. Additionally, genes encoding sucrose symporters, which are typically involved in sucrose export, are expressed at levels that are 6.4 and 6.9 times higher in leaves than in trichomes of LA1777 and LA4024, respectively (Supplemental Data Set 5). These expression profiles were confirmed by RT-qPCR (Supplemental Table 1). Enrichment analysis demonstrated overrepresentation of genes and proteins involved in plastidic and cytosolic glycolysis in GTs, but this effect was significant only in LA1777 (Supplemental Data Set 6).

Next, we found that transcripts encoding enzymes of the CBB cycle were among the top 2000 highest expressed genes only in the leaf samples of both tomato species but not in their trichomes (Figures 6A and 6B). Here, the difference in transcript levels between leaves and trichomes was significant (Figure 7), with average fold changes within this ontology group being 6.3 (LA1777) and 8.4 (LA4024). These results are consistent with the protein abundances obtained from shotgun proteomics (Supplemental Data Set 5), RT-qPCR of selected CBB cycle genes (Supplemental Table 1), and the metabolite profiles of CBB intermediates (Figure 3). On average, genes encoding photorespiration, which is closely coupled to the activity of the CBB cycle, showed up to 22-fold (LA1777) and 34-fold (LA4024) lower expression and up to 4-fold (LA1777) and 46-fold (LA4024) lower protein levels in GTs compared with leaves of the corresponding species (Figure 4; Supplemental Figures 6 and 7, Supplemental Data Set 5, and Supplemental Table 1). Both at the transcript and protein levels, enrichment analyses revealed strong leaf-specific overrepresentation of signals within the MapMan ontology groups 1.2 PS-photorespiration and 1.3 PS. CBB-cycle (Supplemental Data Set 6). Furthermore, transcripts of carbonic anhydrase showed leaf-specific expression and higher protein abundance in leaves than in trichomes (LA1777, 2.8-fold; LA4024, 8.5-fold, $P < 0.05$).

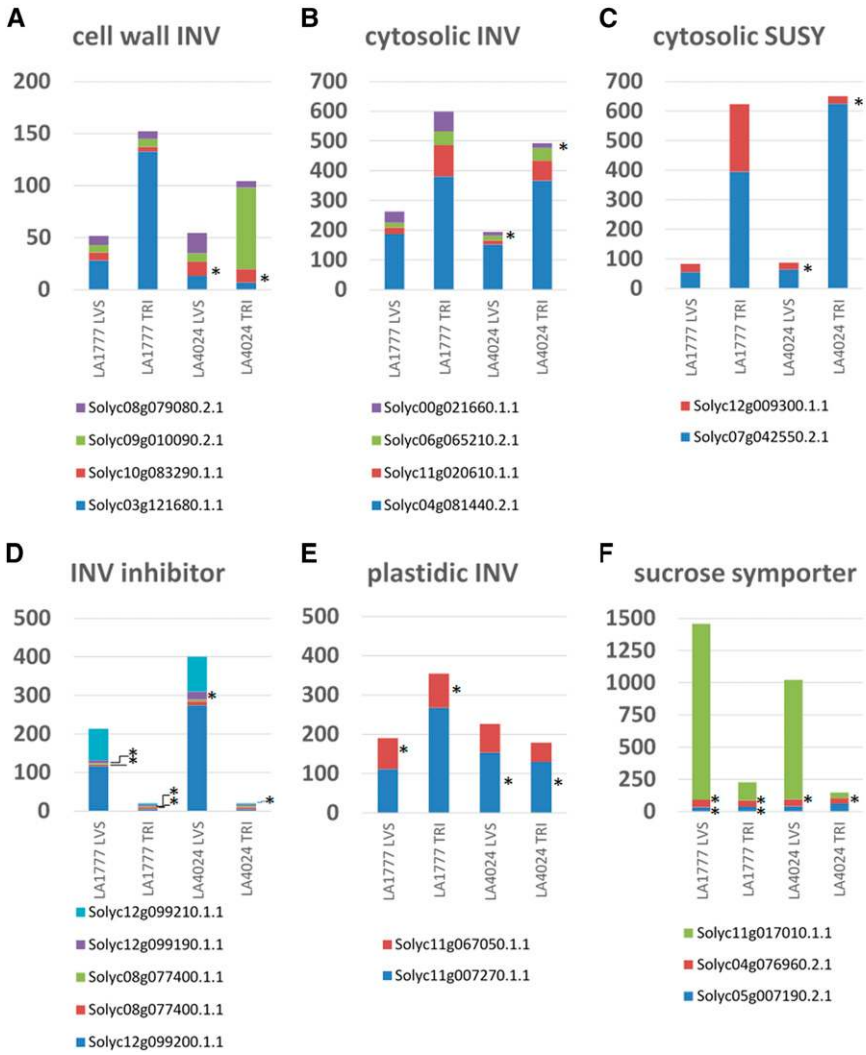

Figure 5. Transcript Profiles of Genes Involved in Sucrose Degradation and Transport in Tomato Leaves and Trichomes.

(A) Cell wall invertases.
(B) Cytosolic invertases.
(C) Cytosolic sucrose synthases.
(D) Invertase inhibitors.
(E) Plastidic invertases.
(F) Sucrose symporter.
Data presented are normalized fluorescence counts from the microarray data (see details in Supplemental Data Set 5). All leaf versus trichome differential expression within a species are significantly different (Student's *t* test $P < 0.05$) except those annotated by an asterisk.

Paralleling lower ADP-glucose levels in GTs, glucose-1-phosphate adenylyltransferase, a unidirectional starch biosynthesis enzyme, showed significantly lower transcript (2- and 3-fold) and protein (13- and 57-fold) levels in GTs of both species compared with their leaves (Figure 7; Supplemental Data Set 5). Likewise, starch metabolism was overrepresented at the transcript level in the leaves of both tomato species (Supplemental Data Set 6).

By contrast, genes of PSI and PSII represented the ontology class with the highest expression levels in all samples (leaves and trichomes of both species). Although expression levels were higher in leaves for most of the highly abundant PSI and PSII genes, these levels differed by <2-fold when comparing trichomes and leaves (Figures 6C and 7; Supplemental Data Set 5). Since many PS proteins are integrated in membranes, they could not be reliably detected by the proteomics method used.

^{13}C-CO_2 and Glucose Labeling Confirm Glandular Trichomes as Sink Organs

^{13}C-labeling of LA1777 with ^{13}C-CO_2 showed significantly slower incorporation of ^{13}C-isotopes into 3-phosphoglycerate (3-PGA) and ribulose-1,5-bisphosphate (RU-1,5-BP) despite smaller pool

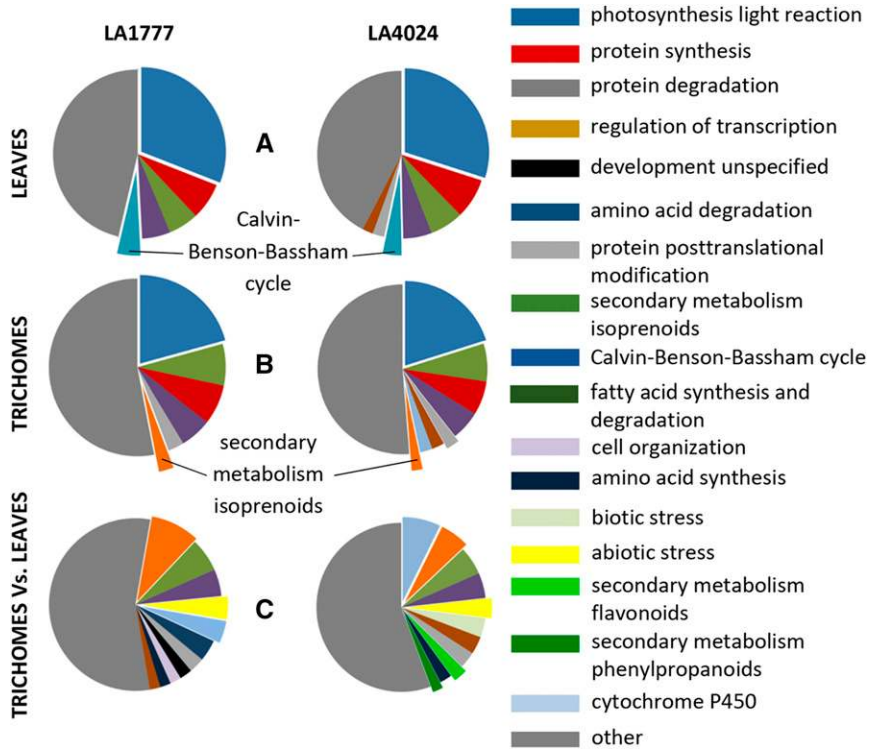

Figure 6. Distribution of the 2000 Most Highly Expressed Genes in Ontology Groups in Leaves, Trichomes, and Trichomes versus Leaves.

(A) and **(B)** For leaves **(A)** and trichomes **(B)**, the 2000 most highly expressed genes were grouped according to MapMan ontology. The categories that represent <2% of the cumulative expression of these 2000 genes were grouped together under "other."

(C) As in **(B)**, except the 2000 top expressed genes are those with a fold change in expression of over 2 in GTs versus leaves. For detailed information, see Supplemental Data Set 5. All data are based on the average of $n = 3$ individual hybridizations per group.

sizes in trichomes versus leaves (Figure 8A). For example, after 10 min, the percentage of labeled C in RU-1,5-BP is only 8% in trichomes, versus 68% in leaves. Because the pool size is smaller in GT, in absolute amount of C, this represents a 32-fold higher incorporation of CO_2 in leaves versus trichomes. In contrast to the CBB intermediates, the fraction of label in sucrose in the trichomes is not significantly different to that of leaves after 10 min and 31% versus 50% in the leaves after 30 min (Figure 8A). Also, in absolute amounts (based on peak area), the incorporation of label in sucrose in trichomes is much higher than that in RU-1,5-BP, indicating that in GT sucrose must be largely imported from the leaves. The pattern distribution of heavy isotopologs in sucrose was similar for leaf and trichome but the ^{13}C enrichment in trichomes lagged behind the ^{13}C-enrichment observed in the leaf (Supplemental Figure 8A and Supplemental Data Set 7, standard deviation isotopologs). Similar enrichment of 3-PGA (68% after 10 min and 84% after 30 min) and RU-1,5-BP (68% after 10 min and 81% after 30 min) with ^{13}C demonstrates that the CBB cycle in leaves is largely fed by atmospheric CO_2 (Figure 8A). By contrast, in GTs, stronger enrichment with ^{13}C of 3-PGA (22% after 10 min and 44% after 30 min) than of RU-1,5-BP (8% after 10 min and 32% after 30 min) upon ^{13}C-CO_2 labeling is observed. This indicates that the label in 3-PGA in part comes from the breakdown of labeled sucrose imported from the leaf.

Labeling with U^{13}C-glucose in ambient CO_2 atmosphere resulted in intensive incorporation of ^{13}C-label in sucrose (Figure 8B). Here, ^{13}C enrichment in the trichomes lagged behind that observed in leaves. Interestingly, the labeling pattern of ^{13}C-isotopologs was similar between leaves and trichomes, particularly at the later time points (Supplemental Figure 8). Among the heavier isotopologs, the signatures of 6x^{13}C and 12x^{13}C most strongly contributed to the labeling patterns in leaves and trichomes, which can be interpreted as direct incorporation of U^{13}C-glucose into sucrose by sucrose-phosphate synthase in the leaves and transport of such labeled sucrose into the trichomes. The fraction of label in the leaves in 3-PGA and RU-1,5-BP is lower than with ^{13}C-CO_2, reflecting the incorporation of ambient ^{12}C-CO_2 (Figure 8B). Nonetheless, significant incorporation of label could be observed in CBB intermediates, indicating replenishment of ^{13}C from glucose catabolism. In trichomes, this phenomenon is exacerbated, resulting, for example, in 30% labeled C in RU-1,5-BP after 24 h versus 17% in the leaves (Figure 8B). Thus, despite a lower fixation rate via the CBB in trichomes compared with leaves (Figure 8A), refixation of CO_2 appears to play proportionally a stronger part in trichomes than in leaves. This is further supported by the pattern of labeling, showing preferential enrichment of heavier isotopologs in 3-PGA and RU-1,5-BP in trichomes versus leaves (Supplemental Figure 8).

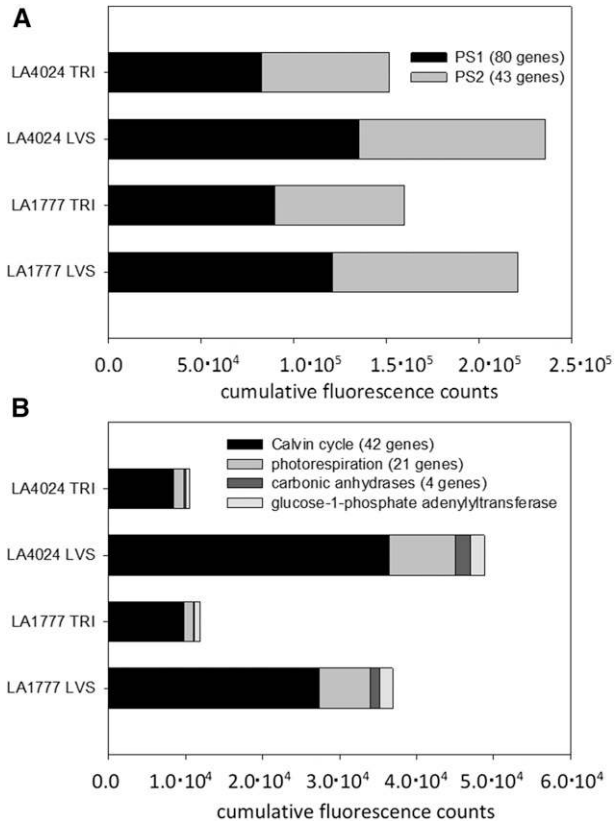

Figure 7. Cumulative Transcript Expression of Photosynthesis Genes.

Light reactions **(A)** and carbon fixation and carbonic anhydrase **(B)**. For details, see Supplemental Data Set 5.

Differential Gene Expression Is Consistent with the Metabolite Spectra Observed in GTs of Wild-Type and Cultivated Tomato

Isoprenoid Biosynthesis Is Highly Active in GTs of Both Tomato Species

Besides protein turnover and RNA regulation, isoprenoid synthesis represented the category with some of the most highly expressed genes in the trichomes of LA1777 and LA4024 (Figure 6). Both species produce high levels of terpenes that are synthesized in the cytosol (sesquiterpenes in both species) (van Der Hoeven et al., 2000) and in the plastids (monoterpenes for *S. lycopersicum* [Schilmiller et al., 2009] and sesquiterpenes for LA1777 [Sallaud et al., 2009]). Therefore, one should expect high level expression of both the mevalonate and the methyl-erythritol phosphate pathways in both species. Genes encoding enzymes of the isoprenoid precursor pathways and the corresponding proteins were strongly enriched in the trichomes (Supplemental Data Set 6) and showed significant trichome-specific expression (Figure 4; Supplemental Figure 9) in both accessions. Accordingly, high expression of genes and proteins of the MEV and MEP pathways as well as high levels of metabolic intermediates of these pathways could be measured (Supplemental Data Set 3). In LA1777 GTs, we note the particularly high levels of methylerythritol-cyclodiphosphate (MEcPP), an intermediate of the MEP pathway, which supplies precursors for the highly abundant sesquiterpene carboxylic acids produced in this species (Figures 3; Supplemental Data Set 3). Since the genes of both the MEV and MEP pathways are overexpressed in GTs, exchange of isoprenyl diphosphate precursors between compartments is unlikely but cannot be excluded.

Amino Acid Metabolism

Although significant in both lines, stronger differences in LA1777 than in LA4024 between trichomes and leaves could be observed with regard to amino acid metabolism (Figure 4; Supplemental Figures 6 and 7). In LA1777 in particular, the metabolism of branched-chain amino acids was upregulated, illustrated by the enrichment analysis of all transcripts (bin 13.4.2.1 in Supplemental Data Set 6) and genes such as those encoding 3-isopropylmalate dehydratase (Solyc03g005730) or 2-isopropylmalate synthase (Solyc08g014230), which is consistent with the higher metabolite levels of valine and leucine/isoleucine (Supplemental Data Sets 3 and 5). Interestingly, genes involved in the degradation of branched-chain amino acids, such as 3-hydroxyisobutyryl-CoA hydrolase (Solyc07g044710), 3-methyl-2-oxobutanoate dehydrogenase (Solyc04g063350), isovaleryl-CoA dehydrogenase (Solyc06g073560), or enoyl-CoA-hydratase (Solyc07g043680), are also overexpressed in GTs (Supplemental Data Set 5). Branched-chain amino acids are precursors of acyl sugars, which are preferentially formed in LA1777 (Slocombe et al., 2008). We also observed high levels of aromatic amino acid decarboxylases in GTs (e.g., Solyc08g066250; Supplemental Data Set 5), whose function is unclear.

Flavonoid Metabolism

Several genes implicated in flavonoid metabolism were upregulated in trichomes with a strong contribution to the biosynthesis of chalcones, flavonols, and dihydroflavonols (Figure 4; Supplemental Figures 6 and 7 and Supplemental Data Set 5). A common pattern in both tomato species is the significant enrichment of transcripts and proteins of the MapMan bin 16.8 (Supplemental Data Set 6), including transcripts encoding proteins such as chalcone synthase (Solyc05g053550) or chalcone-flavonone isomerase (Solyc05g010320). Highest transcript and protein levels were observed in the trichomes of LA4024 as shown earlier in detail for *S. lycopersicum* M-82 (Schilmiller et al., 2010) and correlate well with the large amount of rutin found in trichomes of LA4024, but also for the presence of various methylated myricetin derivatives in both species (Schmidt et al., 2011; Kim et al., 2014).

Lipid Metabolism

In LA1777, 25% ($P = 0.05$) of all transcripts and 56% ($P = 0.01$) of all proteins detected in MapMan bin 11 were significantly upregulated in GTs. In LA4024, 21% ($P = 0.05$) of all transcripts and 49% ($P = 0.01$) of all proteins detected in MapMan bin 11 were

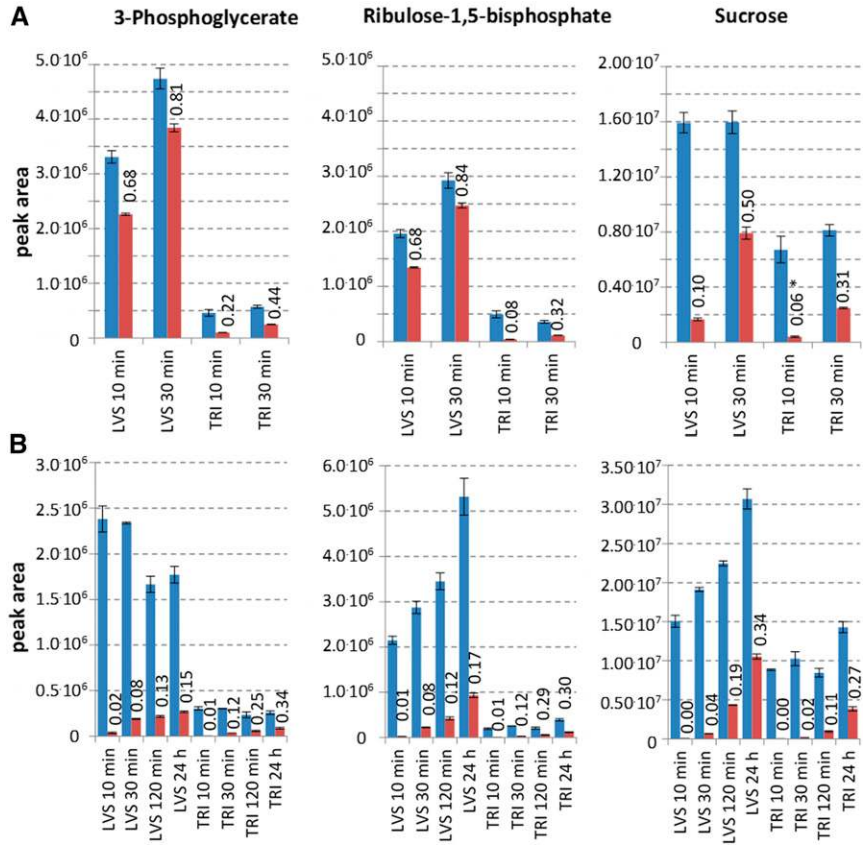

Figure 8. Time Course after ^{13}C-Pulse Labeling of LA1777 with ^{13}C-CO_2 and U^{13}C-Glucose.

^{13}C-CO_2 **(A)** and U^{13}C-Glucose in the presence of ambient CO_2 **(B)**. Blue: total pool sizes of 3-PGA, RU-1,5-BP, and sucrose normalized to sample dry weight. Red: fraction of carbon labeled in these metabolites. Error bars represent the average ± SD ($n = 6$). The fraction of labeled carbon represents the sum of all labeled C from all measured isotopologs. All the data have been corrected for the natural isotopic abundance of ^{13}C-isotopes. Relative isotopolog abundances are presented in Supplemental Figure 8. Numbers above the red bars represent the relative ^{13}C enrichment in the respective metabolites. Differences in the relative ^{13}C-enrichment between leaf and trichome for a given time point are all significant based on heteroscedastic *t* tests ($P < 0.05$) unless indicated by an asterisk.

significantly upregulated in GTs. Furthermore, enrichment analysis showed a marked contribution of genes encoding long fatty acid modification and lipid degradation specific to the GTs of both species (Supplemental Data Sets 5 and 6). Lipid formation in plants normally takes place in the plastids. Therefore, we expected to find transcripts for the plastidic acetyl-CoA carboxylase and malonyl-CoA acyl carrier protein transacylase, the initiating enzymes of fatty acid biosynthesis, both of which are strongly upregulated. However, different subclusters of the acetyl-CoA carboxylase protein complex showed only up to 2-fold higher levels of transcript (e.g., Solyc12g056940) in both species. The transacylase was expressed at relatively low levels in both species and did not show a significant difference between trichomes and leaves (Solyc01g006980). After plastidic biosynthesis of fatty acids with chain lengths of up to C16-C18, extension to longer fatty acids requires their export out of the plastid to the endoplasmic reticulum (Samuels et al., 2008; Kunst and Samuels, 2009). The extension of fatty acids from long (C16 and C18) to very long chains is catalyzed by β-ketoacyl-CoA synthase, β-ketoacyl-CoA reductase, β-hydroxyacyl-CoA dehydratase, and enoyl-CoA reductase (Kunst and Samuels, 2009). Inspection of highly abundant but differentially expressed genes revealed strong upregulation of fatty acid elongases and acyl-CoA ligases in GTs (e.g., Solyc07g043630, Solyc03g031940, Solyc09g083050, and Solyc08g067410; Supplemental Data Set 5). Furthermore, in agreement with the accumulation of polyunsaturated fatty acids in GTs in both species, massive expression was also observed for several trichome-specific desaturases. Solyc11g008680 (log_2-fold change of 4.1 in LA1777; log_2-fold change of 0.53 in LA4024), Solyc01g009960 (log_2-fold change of 3.7 in LA1777; log_2-fold change of 2.83 in LA4024), and Solyc06g059710 (log_2-fold change of 1.5 in LA1777; log_2-fold change of 4.79 in LA4024) encode acyl-carrier protein desaturases. Solyc01g006430 (log_2-fold change of 1.31 in LA1777; log_2-fold change of 1.87 in LA4024) encodes a desaturase of the endoplasmic reticulum and is also upregulated in GTs of both species. High expression of these lipid biosynthesis genes is in good agreement with the measurement of large amounts of

polyunsaturated C18 (in LA4024) and C20 (in LA1777) fatty acids (see above).

Various ROS Detoxification Systems Are Overexpressed in GTs

Photosynthetic oxygenesis, the activity of oxidoreductases, and high metabolic activity in general result in the formation of reactive oxygen species (ROS) such as singlet oxygen. ROS staining in LA1777 indicated much stronger ROS formation in GTs compared with leaf matter (Supplemental Figure 10). Enzymes that are involved in the detoxification of ROS include superoxide dismutase, catalases, and peroxidases for the oxidation of glutathione, ascorbate, or lipids. Very high levels of superoxide dismutase gene expression could be detected in the GTs of both species, with, e.g., Solyc01g067740 belonging to the top 15 most abundant enzymes in the trichomes of both species with protein levels being 31-fold (LA1777) and 39-fold (LA4024) higher than in the leaves (Supplemental Data Set 5).

The high levels of polyunsaturated fatty acids and of oxylipins derived thereof (see above) suggested that these could play a role in the quenching of ROS, as has been shown in other plant systems (Schmid-Siegert et al., 2016). Lipoxygenases represent an essential component of this detoxification pathway, since they consume H_2O_2 and generate lipid peroxides that can be further metabolized. The cumulative gene expression of all 21 lipoxygenases was comparable between leaves and trichomes in both species. Yet, closer inspection of the subcellular localization showed much higher transcript and protein levels for members of the cytosolic LOX1/LOX5 family with 9*S*-lipoxygenase activity. The highest levels were found in GTs of LA1777 (Supplemental Figure 11). By contrast, homologs of the LOX2/LOX3 family in *Arabidopsis thaliana* with 13S-lipoxygenase activity, which are localized in the plastids, were enriched in leaves with one exception (Solyc01g006540). This gene appeared to also be trichome specific in LA4024 and showed one of the highest protein abundances measured of all (Supplemental Figure 11D). These expression results were confirmed by RT-qPCR (Supplemental Table 1).

Furthermore, Solyc07g049690, encoding the fatty acid hydroperoxide lyase, was highly expressed in trichomes of LA1777 and LA4024 with transcript levels being 6 times and 3 times higher and protein abundances being 50 and 150 times higher than in leaves (Supplemental Data Set 5). This finding supports the contribution of lipid oxidation as one important mechanism involved in ROS detoxification. Whereas in leaves expression of hydroperoxide lyase is inducible, in GTs it appears to be constitutively expressed, since no extra environmental stress was applied during our experiments. Altogether, these results are in agreement with the measurements of 9*S*-hydroxy-10*E*,12*Z*-octadecadienoic acid in LA1777 and 13*S*-hydroxy-9*Z*,11*E*-octadecadienoic acid in LA4024.

Lipid hydroperoxides can be recycled by glutathione peroxidases via the oxidation of GSH to GSSG. In both species, most genes encoding GSH peroxidases showed higher transcript levels and higher cumulative protein abundances in trichomes than in leaves and were significantly enriched in the GT protein of both species (Supplemental Figure 12 and Supplemental Data Set 6). The higher GSSG/GSH oxidation state mentioned above is further corroborated by the high expression in GTs of cysteine synthase, which is required for GSH replenishment. Five out of six cysteine synthase-coding genes showed higher expression in trichomes of both tomato lines. Particularly, Solyc01g097940, which dominated the expression of this enzyme family, showed 15- to 17-fold higher transcript levels compared with the corresponding leaves (Supplemental Data Set 5).

In contrast to GSH peroxidases, other enzyme families contributing to the cell redox homeostasis did not show a major upregulation in GTs (Supplemental Figure 12). For instance, glutaredoxins showed similar transcript levels in GTs and leaves of both species, with one isoform-encoding gene (Solyc09g074570) being outstandingly high in the leaves (Supplemental Data Set 5). Among the thioredoxins, with one exception (Solyc05g018700 with transcript levels being 4 to 5 times higher in GTs and moderately abundant protein present only in GTs), similar or lower transcript levels were detected in GTs relative to the leaves of both species (e.g., Solyc07g063190 or Solyc04g081970). With one exception (Solyc04g082460), catalase-coding transcripts were comparable or higher in tomato leaves compared with GTs (Supplemental Data Set 5). Similar or lower transcript and protein levels in GTs compared with leaves in both species were found also for the most abundant ascorbate peroxidases (i.e., Solyc06g005160); thus, the glutathione-ascorbate cycle appears to equally contribute to H_2O_2 removal in GTs and leaves despite the depletion observed for ascorbate in trichomes of LA4024 (Supplemental Data Set 3). Other peroxidases included polyphenol oxidases, which showed GT-specific expression in LA4024 (Solyc08g074620 and Solyc02g078650; Supplemental Data Set 5).

Altogether, our results based on metabolomics, transcriptomics, and proteomics indicate that specific ROS detoxification pathways show increased activity in GTs. In particular, the oxidation of unsaturated lipids and glutathione-based detoxification of reactive peroxides appear to play important roles.

The Metabolism of GTs Is Directed toward the Supply of Precursors and Cofactors for the Major Metabolite Pathways

The abundant biosynthesis of secondary metabolites by GTs requires the supply of carbon from precursors as well as the provision of large quantities of ATP and NAD(P)H. Since the major metabolites in GTs are terpenoids produced from the MEP (plastidic) and the MEV (cytosolic) pathways, it was thus expected that processes delivering triose phosphates and pyruvic acid (for the MEP pathway) or acetyl-CoA (for the mevalonate pathway) are upregulated in GTs of tomato.

Supply of Acetyl-CoA in the Cytosol

Upon glycolysis, acetyl-CoA is produced in the mitochondria. Acetyl-CoA, however, cannot be transported across the mitochondrial membrane. The supply of acetyl-CoA in the cytosol can be achieved via the citrate shuttle (Oliver et al., 2009; Xing et al., 2014). Citrate is transported from the mitochondria or the peroxisomes into the cytosol and cleavage of citrate by the cytosolic ATP-citrate lyase produces oxaloacetate and acetyl-CoA. Microarray expression

data showed that citrate synthases (Solyc01g073740, mitochondrial; Solyc12g011000, peroxisomal) were moderately, but significantly ($P < 0.05$ with *t* test statistics), upregulated in the trichomes of both species (Supplemental Data Set 5), and up to 23-fold higher protein levels were found in GTs relative to the corresponding leaves (Supplemental Data Set 5). Genes encoding ATP-citrate-lyases showed higher transcript levels in LA1777 trichomes and higher corresponding protein levels in GTs relative to leaf matter, supporting citrate export from mitochondria to the cytosol in GTs (Figure 9; Supplemental Data Set 5). Despite the larger pool size of citrate compared with isocitrate, isotopic patterns of citrate after 24 h $U^{13}C$-glucose labeling showed a much higher incorporation of ^{13}C into citrate than was observed for isocitrate (Supplemental Figure 13). In accordance with the smaller citrate pool size in GTs versus in leaves ($P < 0.05$ with *t* test statistics), the ^{13}C enrichment in citrate was more intense in GTs than in leaves. Thus, supporting the transcriptomics/proteomics data, labeling indicates that citrate is largely exported from mitochondria rather than turned into isocitrate via mitochondrial TCA enzymes. Moreover, in contrast to citrate synthase, most other TCA enzymes showed comparable or only slightly increased transcript and protein levels (<3-fold) for trichomes versus leaves of the corresponding line (Supplemental Data Set 5). Our data therefore support the fact that in GTs, the citrate-malate-pyruvate shuttle is used to supply acetyl-CoA in the cytosol, needed to fuel fatty acid elongation, the biosynthesis of isoprenyl diphosphates via the mevalonate pathway, or other key metabolites produced in the cytosol. Higher transcript and protein levels for cytosolic phosphoenolpyruvate carboxykinase (PEPCK), cytosolic pyruvate kinase, cytosolic malic enzyme, and cytosolic and mitochondrial pyruvate dehydrogenase support that carbon withdrawn from the TCA cycle by the ATP-citrate lyase complex is replenished by malate and pyruvate (Figure 9; Supplemental Data Set 5 and Supplemental Table 1). Upregulated transcripts and elevated protein levels of phosphoenolpyruvate carboxylase (PEPC) and PEPCK in GTs indicate that anaplerotic routes to produce oxaloacetate may additionally facilitate the production of cytosolic acetyl-CoA (Tcherkez et al., 2011). For PEPCK, a bidirectional enzyme, preferred carboxylation was demonstrated in C4 plants for high physiological ATP/ADP ratios (Chen et al., 2002). On average, the ATP/ADP ratio (based on peak area) was 1.5 and 2.7 times higher in GTs of LA1777 and LA4024, respectively, compared with the corresponding leaves (Supplemental Data Set 3). This, and increased protein levels of PEPC in GTs versus leaves in both species, also infers that CO_2 is incorporated into oxoaloacetate.

Supply of Pyruvate and Glyceraldehyde-3-Phosphate in the Plastids

The large quantities of plastidic terpenoids produced in GTs of both tomato species (monoterpenoids for LA4024 and sesquiterpenoids for LA1777) indicate that flux through the MEP pathway is important. This is supported by high transcript and protein levels of MEP pathway enzymes in GTs (Supplemental Figure 9, Supplemental Data Set 5, and Supplemental Table 2). Such high MEP pathway flux would require an appropriate supply of its precursors, namely, glyceraldehyde-3-phosphate (GAP) and pyruvate (PYR). Plastidic PYR can be produced via plastidic glycolysis, by plastidic isoforms of malic enzyme, or imported from the cytosol (Oliver et al., 2009; Weber and Bräutigam, 2013; Eisenhut et al., 2015; Shtaida et al., 2015). GAP in the plastids can be supplied by the nonoxidative pentose phosphate pathway, the CBB cycle, by plastidic glycolysis, or by translocation from the cytosol (Flügge et al., 2011).

Plastidic and Cytosolic Glycolysis

Since the subcellular localization of cytosolic and plastidic pools of glycolytic metabolites cannot be unambiguously assigned by metabolomics, it is not possible to conclude whether plastidic or cytosolic glycolysis supplies the carbon for GAP or PYR in GTs based on metabolomics data. Thus, transcriptomics and proteomics results were mined to address this question. Two genes encoding plastidic pyruvate kinases (Solyc01g106780, LA1777, $\log_2$-fold change 3.15; LA4024, $\log_2$-fold change 1.84; Solyc03g007810, LA1777, $\log_2$-fold change 1.80; LA4024, $\log_2$-fold change 2.0) show significantly increased expression in trichomes as well as a gene encoding a plastidic enolase (Solyc03g114500), although in this case differential expression is more pronounced for LA1777 ($\log_2$-fold change 2.3) than for LA4024 ($\log_2$-fold change 0.4) (Supplemental Figure 14, Supplemental Data Set 5, and Supplemental Table 1) in particular at the protein level ($\log_2$-fold change 3.38 in LA1777; no significant change in LA4024). In both species, high transcript levels and protein abundances of several isoforms of fructose-bisphosphate aldolase (FBA) were predicted to be plastidic. Those with the highest expression levels were leaf specific (e.g., Solyc02g062340) and are associated with aldolase activity in the CBB cycle. However, one plastidic FBA (Solyc05g008600) and two cytosolic FBAs (Solyc09g009260 and Solyc10g083570) showed higher transcript and protein levels in trichomes than in leaves with absolute values being high in GTs of both species (Supplemental Figure 14 and Supplemental Data Set 5). Additionally, hexose breakdown in GTs appears to proceed via cytosolic diphosphate-dependent phosphofructokinases, which showed higher expression in GTs compared with leaves (e.g., Solyc04g082880, Solyc12g095760, and Solyc02g081160; Supplemental Figure 14 and Supplemental Data Set 5). Thus, in GTs, provision of triose phosphates seems to be assisted via a combination of cytosolic and plastidic glycolysis. This implies the transport of various sugar and triose phosphates between the cytosol and the plastids.

Other Routes

Alternatively, pyruvate can be produced via decarboxylation of malate by the plastidic NADP-dependent malic enzyme. Genes encoding NADP-dependent malic enzyme, particularly Solyc12g044600, were most strongly expressed in GTs of LA1777 ($\log_2$-fold change = 1.2) and LA4024 ($\log_2$-fold change = 0.3) and also exhibited higher protein levels in GTs versus leaves but only in LA1777 ($\log_2$-fold change = 3.94) (Supplemental Data Set 5). Transketolase, a GAP-producing enzyme involved in the nonoxidative branch of the pentose phosphate pathway, showed high expression of two plastidic isoforms (Solyc10g018300 and Solyc05g050970; Supplemental Data Set 5) of which the latter

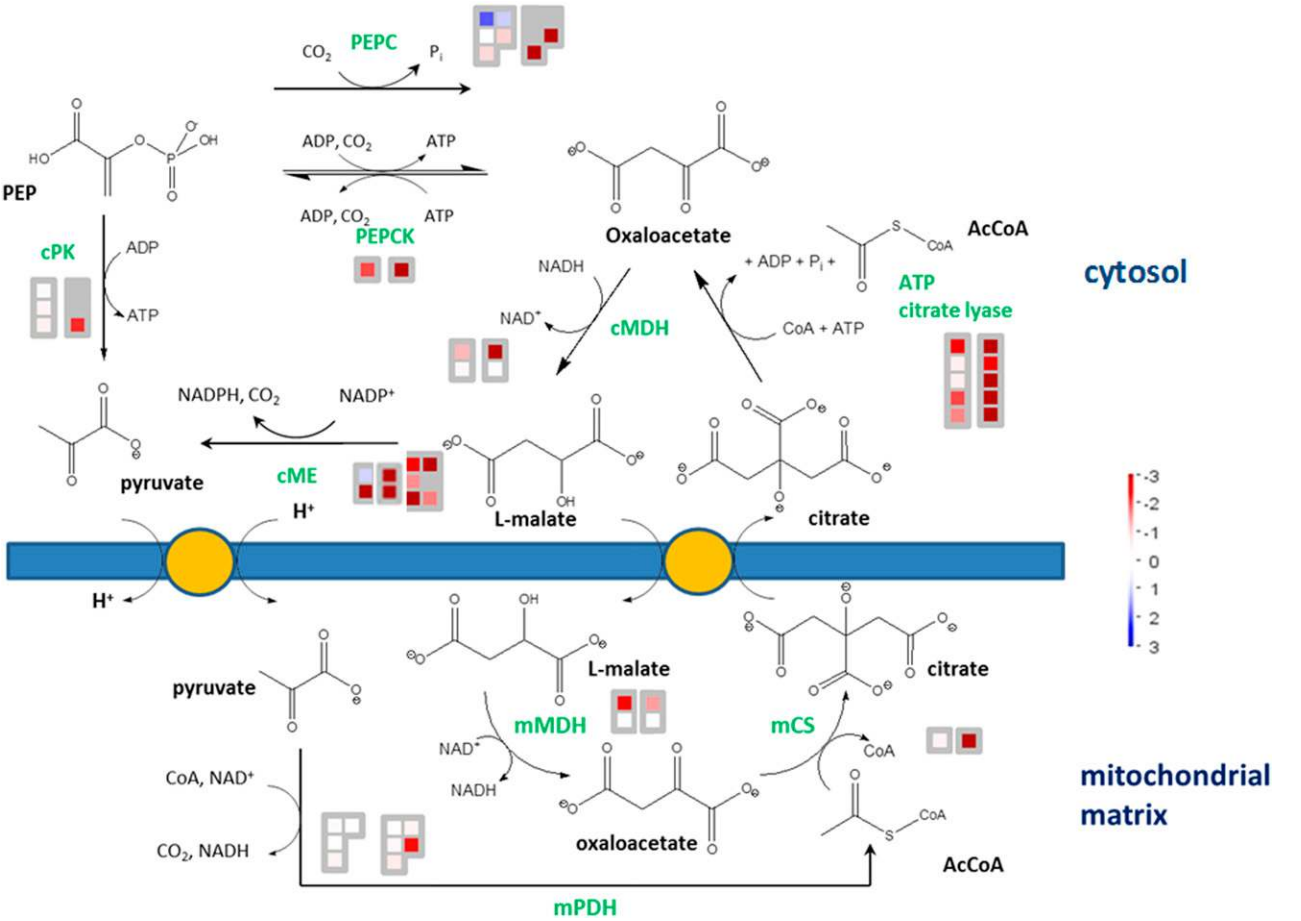

Figure 9. Expression Map of the Citrate-Malate-Pyruvate Shuttle in GTs Compared with Leaves.

Log_2-fold changes between trichomes and trichome-free leaves of LA1777, relative transcript expressions (left boxes) and relative protein abundances (right boxes). Red indicates significant ($P < 0.05$; *t* test) overexpression in trichomes, blue significant overexpression ($P < 0.05$; *t* test) in leaves, and white nonsignificant changes ($P > 0.05$; *t* test). The subcellular localization of the respective enzymes was manually checked using the software tools listed in Methods. The horizontal blue bar represents the mitochondrial envelope and the yellow discs with dark-blue circle the pyruvate-proton symporter (left) and the malate-citrate antiporter (right). cPK, cytosolic pyruvate kinase; cME, cytosolic malic enzyme; cMDH, cytosolic malate dehydrogenase; mMDH, mitochondrial malate dehydrogenase; mCS, mitochondrial citrate synthase; mPDH, mitochondrial pyruvate dehydrogenase.

showed increased transcript levels and protein abundance in GTs of both species compared with the corresponding leaves.

Contribution of the Plastidic Oxidative Pentose Phosphate Pathway

In the oxidative pentose phosphate pathway, glucose-6-phosphate is converted to a pentose phosphate with the release of NADPH. One plastidic isoform of glucose-6-phosphate 1-dehydrogenase (Solyc05g015950) showed elevated transcript levels in GTs (log_2-fold change = 1.7 in LA1777 and 1.09 in LA4024; Supplemental Data Set 5), which was also confirmed by RT-qPCR (Supplemental Table 1), and protein levels were markedly elevated in GTs versus leaves but only in LA1777 (log_2-fold change = 3.89; Supplemental Data Set 5). Furthermore, Solyc12g056120, which encodes a plastidic 6-phosphogluconate dehydrogenase, shows elevated transcript and remarkably high protein levels in trichomes (log_2-fold change = 2.01 in LA1777 and 2.13 in LA4024; Supplemental Data Set 5, SI). High activity of the oxidative pentose phosphate pathway would serve a dual function: to supply NADPH as well as ribulose-5-phosphate for the replenishment of RU-1,5-BP in the CBB cycle.

Transport

The compartmentalization of metabolism implies exchange between compartments, which play an essential role in ensuring appropriate supply of precursors for compartment-specific metabolic pathways. Particularly relevant is the transport of sugar, sugar phosphates, triose phosphates, and carboxylic acids to and from the chloroplasts. The most strongly expressed isoform of the glucose-6-phosphate translocator (Solyc07g064270) is slightly overexpressed in trichomes (log_2-fold change = 1.32 in LA1777 and 0.59 in LA4024), whereas the most strongly expressed isoform of

the phosphoenolpyruvate translocator (Solyc03g112870) shows no differential expression between leaves and trichomes in both species. Triose phosphate translocator Solyc10g008980 showed high transcript levels in GTs of both tomato lines even though the expression level was three times higher in the leaves than in the trichomes (log_2-fold change = 1.27 in LA1777 and 1.53 in LA4024). Triose phosphate translocation in leaves is used to shuttle triose phosphates produced by the CBB cycle from the chloroplasts to the cytosol (Ludewig and Flügge, 2013). However, as glycolytic breakdown of hexose in the cytosol of GTs is indicated by high expression of genes of the top part of the glycolysis pathway, reverse transport of triose phosphate from the cytosol to the plastids would also be plausible. As hexose phosphate is translocated from the cytosol into the plastids of GTs, it can be converted to GAP via plastidic glycolysis or the plastidic pentose phosphate pathway.

Among the putative transmembrane transporters for pyruvate, mitochondrial Solyc10g051120, encoding a putative mitochondrial isoform, was particularly strongly overexpressed in GTs, 2.6-fold in LA1777 (q-value = 1.42×10^{-6}) and 24-fold in LA4024 (q-value = 1.06×10^{-11}), supporting the fact that pyruvate is converted to acetyl-CoA and citrate in the mitochondria, the latter being then exported to the cytosol to be converted to acetyl-CoA by ATP-citrate lyase (see above).

The tomato genome contains several homologs of the bile acid sodium symporter (BASS) family. In Arabidopsis, the BASS2 protein (At2g26900) was shown to function as a plastidial pyruvate sodium-dependent transporter (Furumoto et al., 2011). A phylogenetic analysis of the BASS homologs from Arabidopsis and tomato (Supplemental Figure 15 and Supplemental Data Set 8) indicates a strong conservation of the respective BASS proteins between the species, rather than within species. This suggests that the respective functions of the BASS proteins between these two species are well conserved. The *BASS2* putative ortholog of tomato (Solyc05g017950) shows comparable expression levels in leaves and trichomes in both species, indicating that pyruvate import via BASS2 is not induced in trichomes compared with leaves. By contrast, in LA1777, Solyc08g007590 (*BASS6*) is overexpressed in trichomes (log_2-fold change = 2.05). Arabidopsis has two putative orthologs of Solyc08g007590, *BASS5* and *BASS6*, although it has a higher percentage of sequence identity with *BASS6* than with *BASS5*. Interestingly, *BASS5* (At4g12030) is involved in the transport of methionine-derived alpha-keto acids required for the biosynthesis of the corresponding glucosinolates (Gigolashvili et al., 2009), but the function of *BASS6* is unknown. Since tomato is not known to produce glucosinolates, Solyc08g007590 could be involved in the import of other carboxylic acids with a functional group in the alpha position, for example, C4-dicarboxylic acids such as malate or oxaloacetate. In LA4024, Solyc09g055940 (putative BASS3 ortholog) is overexpressed in trichomes (log_2-fold change = 1.5; P = 0.05). However, the function of *BASS3* is unknown. Its similarity to *BASS5/6* could suggest it is also involved in the transport of carboxylic acids with a functional group in the alpha position. In addition, a homolog of the Arabidopsis dicarboxylic acid transporter (DIT1), Solyc11g065830, shows slight overexpression in trichomes of LA1777 (og_2-fold change = 0.69) but a lower expression in trichomes of LA4024 (log_2-fold change = 2.19).

Supply of ATP and Reducing Power

As for the oxidative pentose phosphate pathway, transcript levels of genes and proteins encoding NADPH-producing enzyme families other than PSI were increased in GTs compared with leaf tissue (Supplemental Figure 16). Thus, in tomato GTs, in addition to NADPH production via photosynthesis, the central carbon metabolism is directed into the production of the reducing cofactor NADPH. On average, the expression of genes in the MapMan ontology group 1.1.4 PS.lightreaction.ATP synthase resulted in transcript levels being 3.4-fold (LA1777) and 3.1-fold (LA14024) higher in leaves than in the corresponding GTs. On the other hand, mitochondrial ATPase transcripts (MapMan group 9.9 mitochondrial electron transport/ATP synthesis.F1-ATPase) were comparable (0.8-fold [LA1777] and 0.8-fold [LA4024]) between leaves and GTs of both species. Thus, photosynthetic ATP and NADPH production in tomato GTs is based on pronounced expression levels of both photosystems (Figure 7). However, its contribution to the energetic homeostasis appears to be lower than in leaves.

DISCUSSION

To identify which metabolic routes deliver energy, reduction equivalents and carbon in tomato GT, we used a multi-omics approach and ^{13}C-labeling experiments. We took advantage of the recent sequencing of the tomato genome for a comprehensive survey of gene and protein expression. The high degree of sequence similarity between LA4024 and LA1777 allowed us to use a single microarray that was designed to hybridize to the RNA of both species. By comparing trichome samples (dominated by type VI trichomes) with nearly trichome-free leaves in two tomato species, we identified metabolic processes that drive the high production of secondary metabolites in this type of GT. As the secondary metabolism in type VI GTs of LA1777 and LA4024 widely overlaps, we only briefly described processes that are specific to either of the lines whenever they contributed to the formation of highly abundant secondary metabolites. The main aim, however, was to emphasize regulatory principles that are common to both tomato models.

Trichome-Specific Central Carbon Metabolism Despite Different Secondary Metabolites

Metabolomics data of secondary metabolites generally confirms earlier works (Besser et al., 2009; Schilmiller et al., 2010; Ghosh et al., 2014). In LA1777 trichomes, the metabolite profile is dominated by short branched-chain acyl sugars with fatty acid chain lengths between C2-C12, flavonoids, free long-chain fatty acids, and sesquiterpene carboxylic acids. In LA4024, the flavanol conjugates dominated the metabolic profile in LC-MS. Beyond these confirmative measurements, to the best of our knowledge, a comprehensive analysis of the central carbon and energy metabolism of GT has not been reported to date. PCA analysis of hydrophilic metabolomes showed that GTs of LA1777 and LA4024 have more in common with each other than with leaves from the same species. This indicates that GTs share unique metabolic processes that relate to their high metabolic activity

despite the different metabolites they produce. The combination of these data with transcriptomics, proteomics, and ^{13}C-labeling data allowed us to extract the salient features of these metabolic cell factories, which will be discussed below, and to integrate them into a metabolic model.

Sucrose Is a Major Carbon Source for GTs

Several arguments support the fact that sucrose is the major carbon source. First, the pool size of sucrose in the leaves is about twice as large as that of trichomes, implying sucrose provision from the leaves via a concentration gradient (Figure 8). Second, the patterns of labeled forms of sucrose were similar for trichomes and leaf matter, especially at later time points. Third, the percentage of labeled isotopologs in GT lagged behind the enrichment observed in leaves during earlier stages. Signals of labeled glucose were low in leaf and trichomes, implying a rapid conversion of glucose into sucrose in the leaf. Instead, incorporation of label was found in sucrose in all 12 positions with the n+12, n+11, n+10, and n+6 isotopologs dominating the signal after ^{13}C-labeling with ^{13}C-CO_2 and the n+6 and n+12 ^{13}C- isotopologs dominating the signal after U^{13}C-glucose labeling (Figure 8; Supplemental Figure 8). In addition, sucrose-degrading enzymes were overexpressed in trichomes in almost all compartments, as shown in Figure 5 for cell wall invertases, cytosolic invertases, and cytosolic sucrose synthase. In parallel, invertase inhibitors were strongly reduced in trichomes, supporting stronger degradation of sucrose in the apoplasm. Sucrose decomposition in nonphotosynthetic GTs of other plant families displayed relatively high enrichment in EST libraries, for instance in peltate trichomes of basil (*Ocimum basilicum*; Gang et al., 2001). From this, it was proposed that carbon of abundant phenylpropenes originates from sucrose imported from the underlying leaves (Gang et al., 2001). In spearmint (*Mentha spicata*), several transcripts encoding enzymes for sucrose catabolism were expressed more in nonphotosynthetic peltate GTs than in trichome-free leaf matter (Jin et al., 2014). In tobacco (*Nicotiana tabacum*), which like tomato has photosynthetic glandular trichomes, high Rubisco activity was indicated by representation in EST libraries and expression levels measured by RT-qPCR (Cui et al., 2011). Besides Rubisco, carbohydrate metabolism represented more than 10% of all proteins defined by the Gene Ontology in a trichome-specific cDNA library of tobacco trichomes. Because GTs of tomato also express photosynthesis genes (for both photosystems and carbon fixation) at high levels, the fact that sucrose constitutes a major carbon source raises the question of the contribution of photosynthesis to C supply in trichomes.

Uncoupling Light Photosynthesis from the Dark Reactions

In GTs, genes encoding proteins of both photosystems were expressed at roughly half the values observed for leaves but had still the most abundant transcripts in GTs, implying that both photosystems are highly active in GTs in delivering ATP, NADPH, and O_2. By contrast, genes for the CBB cycle and photorespiration were 4 to 5 times lower in trichomes compared with leaves. This indicates that there is an uncoupling of gene expression between light photosynthesis and carbon fixation mediated by the CBB cycle in GTs. Consistent with this, genes for starch biosynthesis and degradation are also downregulated in GTs, showing that carbon that is incorporated in GTs is not stored as starch. The lower activity of the CBB cycle in GTs was confirmed by our ^{13}C labeling experiments, which indicated that some CO_2 is fixed via the Rubisco complex, but a large part of the ^{13}C-label was acquired indirectly after supply and breakdown of sucrose and not directly from the atmosphere. That little atmospheric CO_2 is fixed in GTs is further corroborated by the presence of an envelope (cell wall and cuticle), which is even thicker than that of epidermal cells and likely to significantly restrict gas exchange (Figure 1).

The high metabolic activity of the glandular cells requires high levels of chemical energy and reducing power. For example, the plastidic MEP pathway requires 1× ATP, 1× CTP, and 2× NADPH, and the cytosolic mevalonate pathway requires 3× ATP and 2× NADPH to generate one C5 body. One can therefore assume that the energy and reducing power resulting from the activity of the photosystems in GTs support this high metabolic activity. The uncoupling of light photosynthesis from the dark reactions raises the issue of the function of the CBB cycle in GTs. Despite the lower expression of CBB cycle genes in GTs compared with the leaf, their expression is far from negligible. The most strongly expressed Rubisco small subunit isoform (Solyc02g085950) still ranks among the top 350 most highly expressed genes in GTs of LA1777 and LA4024. CO_2 produced internally in the trichomes is potentially recycled via the activity of Rubisco without a full CBB cycle, as previously shown in developing green *Brassica* seeds (Schwender et al., 2004). In our ^{13}C-U-glucose labeling experiments, RU-1,5-BP and 3-PGA display stronger ^{13}C enrichment in trichomes than in leaves, particularly with heavier isotoplogs (e.g., n+4 and n+5 for RU-1,5-BP and n+3 for 3-PGA) (Figure 8; Supplemental Figure 8). This implies that in trichomes the CBB cycle is replenished via sucrose breakdown products. This could be accomplished through the supply of C5 units from the oxidative pentose phosphate pathway or through glycolytic formation of triose phosphates, both of which are overexpressed in trichomes.

Elevated Lipid Metabolism and Lipid Oxidation Are Common Features in GTs: Hydroperoxide Lyase Is Coexpressed with Genes of the MEP Pathway

Tightly connected to active photosystems and the activity of oxidoreductases is the formation of ROS, the presence of which was substantiated by ROS staining experiments (Supplemental Figure 10). Our data (both metabolite and gene expression) point to the activation of mechanisms that provide increased protection against oxidative stress in GTs. First, we see high levels of unsaturated fatty acids (C20:4 in LA1777 and C18:3 in LA4024) and high levels of oxidized derivatives of these PUFAs. Next, we see high expression of genes encoding lipoxygenases and hydroperoxide lyase, indicating lipid peroxidation activity. Interestingly, hydroperoxide lyase was shown to be induced by high levels of MEcPP via retrograde signaling from plastid to nucleus (Xiao et al., 2012). Moreover, abiotic stresses robustly modulated MEcPP levels and thus induced hydroperoxide lyase expression. As in hydroxy-methyl-butenyl-diphosphate-synthase (*HDS*; EC 1.17.7.1) mutant lines of Arabidopsis, high

levels of MEcPP also coincided with high hydroperoxide lyase transcription in GTs. However, whether high hydroperoxide lyase expression in GTs is the result of high MEcPP levels remains to be demonstrated. The strong upregulation of GSH peroxidase and other peroxidases was also observed in tomato GTs contributing to the detoxification of ROS. The induction of similar processes that cope with ROS has also been observed in trichomes from other species. For example, strong upregulation of lipid and glutathione metabolism was shown in *A. annua* and mint trichomes (Soetaert et al., 2013; Jin et al., 2014). Soetaert et al. (2013) also showed that, as in tomato, nonplastidic elongases and desaturases as well as glutathione metabolism were strongly elevated in GTs of *A. annua*. Thus, detoxification of ROS by high levels of peroxidases and lipoxygenation seem to be a trichome-specific feature.

Increased Supply of Precursors for Secondary Metabolite Pathways in GTs

Tomato GTs produce large quantities of terpenoids both from the cytosolic MEV and the plastidic MEP pathways. Therefore, it is to be expected that the metabolites that are at the origin of these pathways should also be supplied in adequate amounts. The precursor of the MEV pathway is acetyl-CoA. Our data support a strong induction of the citrate-malate-pyruvate shuttle system, which allows the synthesis of acetyl-CoA in the cytosol. A key element of this shuttle is the cytosolic ATP-citrate lyase, which cleaves citrate exported from the mitochondria to acetyl-CoA and oxalo-acetate. ATP-citrate lyase is strongly enriched in trichomes (Figure 9), as are a number of enzymes typically associated with this shuttle system. Recently, Xing et al. (2014) highlighted the central role of ATP-citrate-lyase in the production of cutin and acetyl-CoA-derived polyhydroxybutyrate in transgenic Arabidopsis. Thus, the overexpression ATP-citrate lyase together with a number of enzymes involved in this process constitutes a potential engineering target for increasing flux through the MEV pathway.

The precursors of the MEP pathway are PYR and GAP. Both are intermediates of glycolysis, which can take place either in the cytosol or in the plastids. Several genes encoding plastidic isoforms of enzymes of the lower part of the glycolysis pathway, such as pyruvate kinase and enolase, were overexpressed in GTs. Since some enzymes of glycolysis are also shared by the CBB cycle, which is overall significantly downregulated in GTs, it is of interest to see how specific isoforms are expressed in GTs. Thus, Solyc05g008600, which encodes a predicted plastidic FBA, is overexpressed in trichomes and shows the opposite trend as other genes encoding plastidic FBAs. Therefore, there is a strong indication that plastidic glycolysis is fully expressed in GTs. MEP pathway precursors could also be provided by other means, for example, via the CBB cycle, which although downregulated in trichomes, is still active and can supply GAP. Furthermore, we also note the increased expression of glucose-6-phosphate and triose phosphate plastidic transporters in GTs, indicating that G6P and triose phosphates represent important carbon supplies to the chloroplasts of GTs. Another potential source of precursors for the MEP pathway comes from C4 dicarboxylic acids. Particularly in LA1777, we noted a significant overexpression of a plastidic isoform of NADP-dependent malic enzyme (Solyc12g044600). Malic enzyme converts malate to pyruvate, thereby releasing CO_2 and NADPH. High levels of malate in the plastids would require transport of malate from the cytosol to the plastids. Of the characterized dicarboxylic acid transporters, only one (Solyc11g065830) showed moderately increased expression levels in trichomes, but several genes annotated as encoding mitochondrial carrier proteins (e.g., Solyc05g052640), which have homology to yeast mitochondrial dicarboxylic acid transporters, show strong expression in GT. The exact function of these transporters in plants is not known, and it is tempting to speculate that they might be involved in the import of dicarboxylic acids into the plastids in the context of cells with low CBB activity. Also of interest is the overexpression of genes coding for transporters of the BASS family, Solyc08g007590 in LA1777 and Solyc09g055940 in LA4024, which are putative orthologs of BASS6 and BASS3, respectively. The function of these transporters in Arabidopsis is not yet known, but BASS5, which is closely related to BASS6, is involved in the transport of methionine-derived α-ketoacids, suggesting BASS6 and BASS3 are also potential candidates for the transport of C4-dicarboxylic acids, such as malate. In connection to C4 metabolism, high levels of expression of PEPC in LA1777 trichomes and of PEPCK in the trichomes of both species were observed. Although PEPC is well established as a CO_2 fixating enzyme, PEPCK is typically regarded as a decarboxylating enzyme. However, PEPCK is a bidirectional enzyme and preferred carboxylation was demonstrated in C4 plants for high physiological ATP/ADP ratios (Chen et al., 2002), which is the case in tomato GTs. Thus, high expression of PEPC and PEPCK could indicate a transient CO_2 fixation in the form of C4 dicarboxylic acids, which when transported to the plastids would be further converted to pyruvate. CO_2 released by this reaction could then be recycled by Rubisco, thereby increasing the carbon efficiency of the glandular cells. Thus, it appears that the supply of pyruvate and glyceraldehyde-3-phosphate for the MEP pathway is supported by several processes involving plastids and the cytosol. GTs of LA1777 and LA4024 produce terpenes that are synthesized in the cytosol (sesquiterpenes in LA4024 and LA1777) and in plastids (monoterpenes in LA4024 and sesquiterpenes in LA1777). This raises the question of the crosstalk between the MEV and MEP pathways in GTs, a phenomenon that has been observed previously in several plant systems (Dudareva et al., 2005; Lipko and Swiezewska, 2016). Our transcriptomics and proteomics data (Supplemental Figure 9) indicate that both the MEV and MEP pathways are highly active in GTs, particularly in LA1777, in agreement with the higher terpene productivity in this species. From this, it can be concluded that each of the isoprenoid precursor pathways likely supplies precursors for the terpenes that are produced in their respective compartment. However, it is not possible to exclude the transfer of precursors from one compartment to the other with the available data. This would require labeling with, for example, deuterated deoxyxylulose or mevalonolactone.

The comparison between LA4024 and LA1777 indicates many similarities in GTs but also some differences. Some notable features are the higher expression of genes in the MEP pathway, the plastidic glycolysis (enolase and pyruvate kinase), or the

plastidic NADP-malic enzyme in LA1777, which likely contribute to a higher flux in the plastidic isoprenoid pathway in that species. This is consistent with the significantly higher productivity of GTs in LA1777 (97 times more terpenoids produced than in LA4024).

A Model for Glandular Trichome Metabolic Efficiency

Integrating these observations, we propose a model on how primary metabolism in tomato type VI GTs is organized to supply adequate amounts of precursors for the major metabolic output, which consists essentially of terpenoids in LA1777 (Figure 10). Sucrose imported from the leaves constitutes the major carbon source. The light-dependent reactions of photosynthesis supply energy and reducing power for the metabolic activity, although a major difference with mesophyll cells is that the energy and reducing power are not used primarily for carbon fixation via the CBB cycle, but for the secondary metabolite pathways, principally terpenoid and lipid biosynthesis. A possible contribution of the

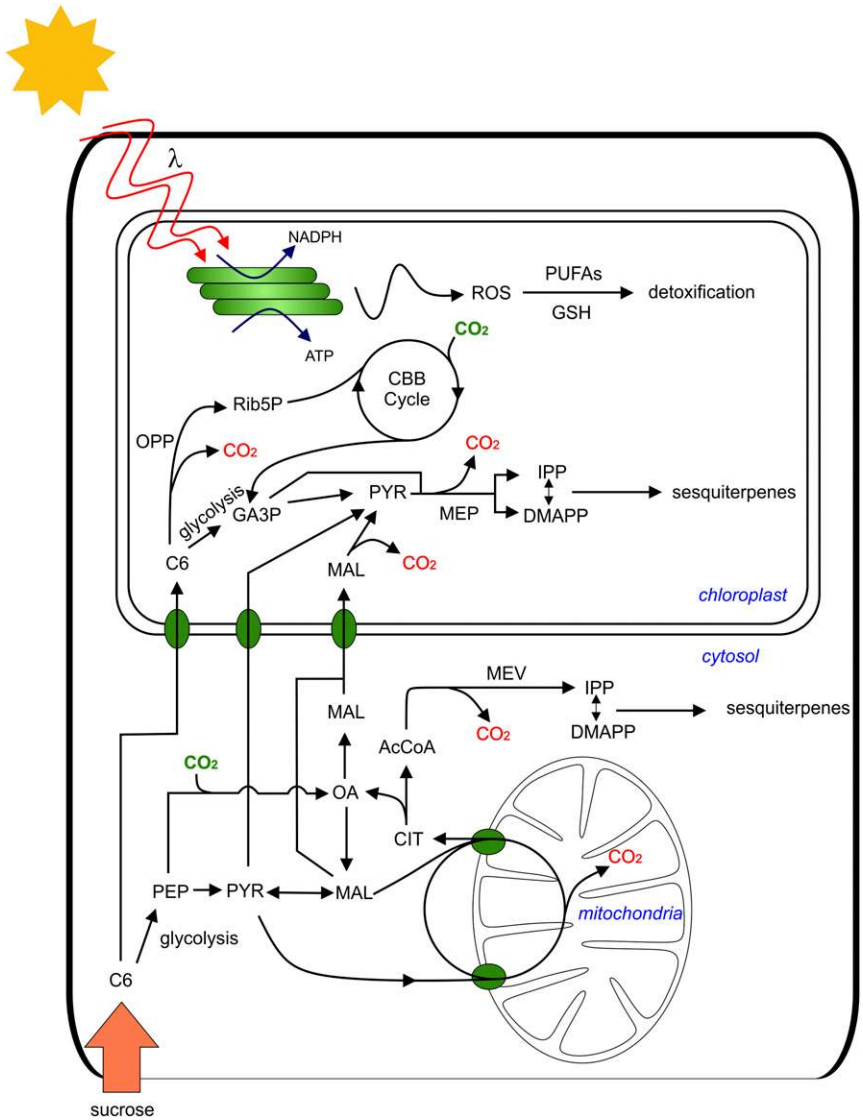

Figure 10. A Putative Model of Central Carbon and Energy Metabolism in Tomato GTs.

A type VI glandular cell with its plasma membrane as a black line. The three main compartments involved (chloroplast, cytosol, and mitochondria) are indicated in blue. The yellow star represents the sun, which emits light of photosynthetically active wavelengths (λ). These allow the photosystems in thylakoid membranes (represented by stacks of green horizontal bars) to produce chemical energy (ATP) and reducing power (NADPH). Photosynthesis and metabolic activity are accompanied by the production of ROS, which are detoxified by PUFAs and glutathione. CO_2 is in red in reactions where it is released and in green in reactions where it is fixed. Black arrows between metabolites represent either metabolic pathways or reactions that are discussed in detail in the main text. AcCoA, acetyl-CoA; C6, hexose; CIT, citrate; DMAPP, dimethylallyl diphosphate; GA3P, glyceraldehyde-3-phosphate; IPP, isopentenyl diphosphate; MAL, malate; OA, oxaloacetate; OPP, oxidative pentose phosphate pathway; Rib5P, ribulose-5-phosphate.

CBB cycle is refixation of CO_2 generated by the metabolic activity, thereby increasing the carbon efficiency. The photosynthetic activity generates ROS, which are dealt with by oxidation of PUFAs and other antioxidant mechanisms such as superoxide dismutase or glutathione peroxidases. The direct supply of precursors for isoprenoid biosynthesis is supported by the increased expression of specific enzymes. For acetyl-CoA in the cytosol, the citrate-malate-pyruvate shuttle, including ATP-citrate-lyase, appears to play a key role, while for GAP and PYR in the plastids, several sources are likely. Plastidic glycolysis probably plays a major role, but the recycling of metabolic CO_2 through Rubisco and replenishment of carbon units from the oxidative pentose phosphate pathway could contribute significantly to the CBB cycle. Additionally, PYR and reducing power can be produced by the activity of the plastidic malic enzyme from malate. However, this also requires the presence of plastidic malate as well as a reflux of C4-units from the cytosol into the plastids. Since the low expression of known C4 translocators does not correspond with the observation of highly expressed plastidic malic enzyme, the existence of novel, yet undiscovered, C4 transporters is anticipated.

Our model provides an initial framework for understanding these metabolic cell factories. Evaluating the contributions of individual enzymes to the global carbon and energy balance of these cells will be the focus of subsequent work. This model also provides some novel clues for applications in metabolic engineering of isoprenoids by transposing the knowledge to other systems, for example, to yeast or microalgae.

METHODS

Plant Growth

LA4024 and LA1777 seeds were obtained from the Tomato Genetics Resource Center, UC Davis, CA. Plants were grown in the greenhouse on soil in the following conditions: 65% humidity, in addition to sunlight artificial light generated by MT250DL metal halide lamps with an intensity of 165 μmol s^{-1} mm^2 (16-h light period), 25°C) and watered with tap water every 2 d. Once a week the plants were treated with a fertilizer solution (0.1% Kamasol Brilliant Blau; Compo Expert). Plant material was harvested 12 and 14 weeks after sowing during the light phase in the early afternoon.

Harvest of Trichome and Leaf Material

For trichome harvest, which always took place at around noon, 20- to 30-cm-long tomato leaves cut one by one were placed in the palm of one gloved hand and exposed to the light, and trichomes were quickly (in <5 s) brushed off the leaflets (around 5 cm each) with a 2-cm broad paintbrush that had been dipped in liquid nitrogen as described by Balcke et al. (2014). Each of the three biological replicates was composed of leaves of 15 plants for LA1777 and 50 plants for LA4024. For each biological replicate, the leaves were cryo-brushed as described above, resulting in a pool of trichomes. A subset of the brushed leaves devoid of trichomes was likewise used to make a pool of leaves. Both pooled trichomes and pooled trichome-free leaves were immediately collected in mortars filled with liquid nitrogen. The crude quenched trichome fraction was further enriched under liquid nitrogen conditions by sieving through steel sieves of 150-μm mesh width (Retsch) (Balcke et al., 2014). Trichome-free leaves were gently ground in a mortar likewise filled with liquid nitrogen. After removal of all liquid nitrogen during storage at –80°C, leaves and trichomes were lyophilized overnight for subsequent metabolomics or remained frozen in a deep freezer until use.

Metabolite Extraction

Using wall-reinforced cryo-tubes of 1.6 mL volume (Precellys Steel Kit 2.8 mm; Peqlab Biotechnologie) filled with five steel beads (3 mm), 25 mg aliquots of dry leaf or trichome powder from three independent pools was resuspended in 900 μL dichloromethane/ethanol (–80°C). Then, 200 μL of 50 mM aqueous ammonium acetate buffer (0°C, pH 6.7) was added to each vial and cell rupture/metabolite extraction was achieved by FastPrep bead beating (3 × 20 s, speed 6.5 m/s, first round –80°C, second round room temperature; FastPrep24 instrument with cryo adapter; MP Biomedicals). After phase separation by centrifugation at 20,000*g* (2 min, 4°C), 150 μL of the aqueous phase was collected and the Fastprep beating was repeated after adding another 150 μL of ammonium acetate. After the second centrifugation, another 200 μL aqueous phase was combined with the first extract and 600 μL of the organic phase was collected. Then, 500 μL fresh tetrahydrofuran was added twice to the extraction residue and the Fastprep beating was repeated. Each time, 450 μL tetrahydrofuran extract was combined with the first organic phase extract. The aqueous phase was then lyophilized and the organic phase was dried in a stream of nitrogen gas.

For analysis of hydrophilic intermediates by ion pairing LC-(−)ESI-MS, lyophilized samples of the aqueous phase were dissolved in 150 μL of deionized water and filtrated by centrifugation over 0.2 μm PVDF (96 well, Corning, 450*g*, 5 min, 4°C). For analysis of semipolar intermediates in the organic phase, dried samples were dissolved in 180 μL buffer of 75% methanol and 25% water, filtrated by centrifugation over 0.2 μm PVDF (96 well, Corning, 450*g*, 5 min, 0°C), and processed by reverse-phase LC-(+)ESI-MS and reverse-phase LC-(−)ESI-MS. Detailed chromatography and mass spectrometry parameters are provided in Supplemental Table 3, Supplemental Table 4, and Supplemental Data Set 9.

For analysis of volatile metabolites, surface extracts were collected from six leaflets of ~5 cm length by adding 2 mL *n*-hexane and shaking for 1 min. The hexane was transferred to a clean tube and centrifuged at 16,000*g* for 90 s to remove debris. The hexane extract was then directly injected in the GC.

Metabolite Profiling

Detection Approach, Data Matrix, and Data Normalization

Nontargeted ion detection in LC-MS was achieved using an Acquity UPLC (Waters) and a TripleTOF 5600 mass spectrometer using the software Analyst 1.6 TF (Sciex). Hydrophilic metabolites were separated by ion pairing chromatography (Supplemental Table 3), and semipolar metabolites were separated by reverse-phase UPLC (Balcke et al., 2014). TOF-MS^1 mass features were assayed between 65 and 1250 D simultaneously with an array of nontargeted QToF-MS^2 scan experiments by sequential window acquisition of all theoretical fragment-ion spectra (SWATH)-QToF-MS/MS (Hopfgartner et al., 2012). During the latter, the transmission range for precursor ions in the Q1-quadrupol was set for 20 ms to mass windows of 33 D and was incremented from m/z = 65 to 1250. Simultaneously, CID fragmentation was acquired in relation to each SWATH transmission window. Thus, compromising between Q1 dwell times and MS^2 spectra purity, LC-SWATH-MS/MS measurements allow for rapid assessment of MS^1 and MS^2 spectra with cycle times of below 1 s. In total, LC-SWATH-MS/MS resulted in 8308 MS^1 distinct mass/retention time features with reliable CID fragmentation (3833 aqueous phase; 3475 from the organic phase). Out of all LC-MS features, we assigned the structure of 243 metabolites by comparison to the retention time, exact mass (MS^1), and CID fragmentation pattern (MS^2) of authentic standards (Supplemental Data Sets 1 to 3). All data presented were normalized to dry weight. Since

secondary metabolites of GT contribute significantly to the dry weight of GTs, which is not the case in leaves, normalization based on dry weight to compare different plant organs may bias the conclusions made. Therefore, other normalization approaches were tested including normalization to the total nitrogen content thought to represent the total pool of proteins and nucleic acids. Based on this normalization, however, similar trends were observed and we chose to present the data normalized to dry weight.

If authentic standards were not available, we predicted the metabolite identity or affiliation to a class of secondary metabolites by exact mass, isotopic distribution of carbon in MS^1 spectra, CID fragmentation patterns, and the plausibility of the metabolite appearance and retention time in the chromatogram of aqueous or organic extracts. All LC and MS parameters and a list of used authentic standards are given in Supplemental Data Sets 1 to 3 and 9, and Supplemental Tables 3 and 4.

Volatile metabolites were measured from 1 μL of the hexane supernatant by GC-MS on a Trace GC Ultra gas chromatograph coupled to an ISQ mass spectrometer (Thermo Scientific). GC-MS analyses were performed according to Brückner et al. (2014).

Estimation of the Rutin, Sesquiterpene Carboxylic Acid, and Terpene Content in GT

Twenty-five milligrams of dry trichome material was exhaustively extracted by 10 consecutive extractions (short vortexing) with a mixture of 75% methanol and 25% water. Aliquots of the extracts were diluted to meet the linear range of the following LC-MS analysis. Rutin (Sigma-Aldrich) and (*E*,*E*)-farnesoic acid (Echelon) pure standards were used for external calibration of Rutin in LA4024 and of two major sesquiterpene carboxylic acids [(+)-(*E*)-α-santalene12-oic acid and (+)-(*E*)-endo-bergamotene-12-oic acid] in LA1777 trichome extracts. Since the latter compounds were both not commercially available, we assumed the same MS response as with farnesoic acid. For the estimation of terpene content in LA4024, leaf surface extracts were prepared from ~1.5-cm-long leaflets in three consecutive extractions with hexane containing dodecane at a concentration of 0.15 mg L^{-1} and measured by GC-MS as described above. The concentration of the terpenes was estimated by adding the peak area of the five major monoterpenes detected and using the peak area of dodecane as a reference.

Shotgun Proteomics

Protein Extraction and Trypsin Digestion

One-hundred milligrams of frozen, powdered tomato trichomes or leaves (three independent pools each) was washed with 10% TCA in acetone followed by acetone both at –20°C. The tissue pellet was suspended in 400 μL of extraction buffer (100 mM Tris-HCl, pH 8.5, 1% [w/v] SDS, 25% [w/v] sucrose, 5 mM EDTA, 0.5% [v/v] β-mercaptoethanol, and 1% plant protease inhibitor cocktail [Roche]), both added fresh, and the suspension was mixed vigorously for 30 min at room temperature. An equal volume of water saturated phenol was added and the homogenate was further mixed for 30 min. The homogenate was centrifuged at 10,000*g* for 10 min at room temperature. An equal volume of reextraction buffer (100 mM Tris-HCl, pH 8.5, 20 mM KCl, 25% [w/v] sucrose, 10 mM EDTA, and 0.5% [v/v] β-mercaptoethanol added fresh) was added to the top phenol phase. The homogenate was mixed vigorously for 15 min at room temperature and centrifuged as described above. Proteins were precipitated from the phenol phase with 5 volumes of –20°C 100 mM ammonium acetate in methanol overnight. Proteins were collected by centrifugation, washed two times with 20% 50 mM ammonium bicarbonate and 80% acetone, and dissolved in 8 M urea and 50 mM ammonium bicarbonate. The concentration of the protein solution was measured using the 2-D Quant Kit (GE Healthcare) following the manufacturer's instructions. Disulfide bonds were reduced with 200 mM DTT, 100 mM Tris-HCl, and alkylated with an excess of 200 mM iodoacetamide and 100 mM Tris-HCl. Proteins were digested with trypsin (enzyme to protein ratio 1:50) at 37°C overnight. The peptide solution was desalted with C18 reverse-phase batch chromatography in STAGE tips. The C18 matrix was conditioned with 80% acetonitrile (ACN) and 0.1% formic acid (FA) in double-distilled water and equilibrated with 0.1% FA in double-distilled water. Retained peptides were washed with 0.1% FA in double-distilled water and eluted with 80% ACN and 0.1% FA in double-distilled water. Peptides were dried in a vacuum concentrator and dissolved in 5% ACN and 0.1% TFA.

Liquid Chromatography and Mass Spectrometry

Four micrograms of peptides was injected into an EASY nLC1000 liquid chromatography system from Thermo Fisher Scientific. Peptides were separated using C18 reverse-phase chemistry on an EASY-column SC001 precolumn (length 2 cm, inner diameter 100 μm, particle diameter 5 μm) in-line with an EASY-Spray ES803 column (length 50 cm, inner diameter 75 μm, particle diameter 2 μm) both from Thermo Fisher Scientific with a gradient from 5 to 40% acetonitrile in 9 h and a flow rate of 250 nL/min. The column temperature was set to 40°C. Peptide ions were electrosprayed on-line into an LTQ Orbitrap Velos Pro mass spectrometer via an EASY Spray ion source both from Thermo Fisher Scientific. The spray voltage was 1.9 kV, the capillary temperature was 275°C, the S-lens RF level was 50%, the multipole offset was −7 V. Full MS survey scans of the total ion population were performed with a resolution of 60,000 in the Orbitrap mass analyzer. The automatic gain control target value was 10^6; the maximum injection time (maxIT) was 500 ms, and 1 microscan was acquired. Full scans were followed by up to 20 data-dependent (DDA) MS/MS scans of the most abundant precursor ions with a minimum signal threshold of 500 fragmented using CID in the LTQ mass analyzer. The automatic gain control target value was 10^4; the maxIT was 200 ms, and 1 microscan was acquired. The dynamic exclusion repeat count was 1, the repeat duration was 30 s, the exclusion duration was 240 s, and the exclusion mass width was ±10 ppm. Mass spectra were calibrated internally in real time using the *m/z* 445.120024.

Peptide and Protein Identification and Quantification

Peptide spectral matches (PSMs) were generated with Mascot software v2.4.0 from Matrix Science linked to Proteome Discoverer v1.4 (PD) from Thermo Fisher Scientific. A signal-to-noise threshold of 1.5 was used to filter ion signal peaks from MS full scans. The International Tomato Annotation Group (ITAG) release 2.3 of the tomato proteome database amended with common contaminants (34,727 sequences; 11,956,401 residues) was searched with a precursor ion tolerance of 7 ppm, a fragment ion tolerance of 0.8 D, enzyme setting trypsin, two tolerated missed cleavages, and carbamidomethylation of cysteine as a fixed modification. The family-wise PSM error rate was controlled via the false discovery rate (FDR/q-values) using the target/decoy database model for estimating false positive PSMs with the target decoy PSM validator module in PD. Peptides and proteins were identified using the Peptide and Protein Prophet algorithms in Scaffold v.4.0.5. A 95% peptide threshold and an 80% protein threshold were equivalent to a 0.01% peptide FDR and a 0.2% protein FDR. Proteins were quantified using the "Quantitative Value (Normalized Total Spectra)" option in Scaffold.

Transcriptomics

RNA Preparation

Total RNA was isolated from three independent pools of trichome-free leaves and trichome preparations using the Qiagen RNeasy kit. The RNA was DNase treated with the Ambion DNA-free kit, quantified via NanoDrop, and quality assessed using the Qiagen Qiaxcel capillary electrophoresis

system. Only samples with an estimated RIN number of 8 or greater were used for downstream applications.

Microarray

Seventeen mRNA samples from six *Solanum habrochaites* accessions (LA1731, LA1753, LA1777, LA2158, LA2167, and LA2650) and two *Solanum lycopersicum* accessions (LA4024 and LA4005) were sequenced to obtain an average of 59,080,335 single end, 101-bp reads per library (Supplemental Table 5). Reads were aligned to the tomato reference genome version 2.4 using TopHat2 v2.0.6 with the following parameters: –max-insertion-length 9–max-deletion-length 9 -p 8 -g 1–library-type fr-unstranded -m 1–read-gap-length 12–read-edit-dist 12–read-mismatches 8–read-realign-edit-dist 0–no-coverage-search–segment-mismatches 3. An average of 82% of all reads mapped uniquely to the reference, with slightly more reads aligned in the *S. lycopersicum* samples (Supplemental Table 5). For each alignment, duplicated reads were then removed and indels were realigned using Picard v1.65 and GATK v2.2.8 with default parameters. Alignments for all libraries from the same accession were merged, resulting in an average of 103 million reads per accession (range from 74–166 million; Supplemental Table 5). Variants in all alignments were called simultaneously using GATK and the resulting file was used to define a set of exonic regions covered by RNA-seq reads but free of any polymorphism between LA4024 and LA1777. This analysis resulted in 403,328 regions larger than 25 bp distributed across 25,892 out of the 34,727 cDNAs present in the ITAG annotation v2.30. These sequences were provided to Affymetrix, where 398,006 of these sequences were selected to be included in the array. In addition, a number of probes to genotype LA1777 and LA4024 were added to the chip. From the 363,286 SNPs found between these two accessions, we filtered for those that had no other variant in 20 bp on each side and were at least 20 nucleotides away from an exon boundary. This resulted in 14,557 probes containing a single SNP that were also included in the array.

Triplicate microarray hybridizations of leaf and trichome RNA preparations of LA1777 and LA4024 were performed on an Affymetrix GeneAtlas system with the custom-designed microarray chips (see description above). One hundred fifty nanograms of total RNA of each preparation was used as starting template using the Ambion WT Expression Kit, the Gene Chip Eukaryotic Poly A RNA Control Kit, and the Gene Chip WT Terminal Sequencing Kit according to the manufacturer's protocols. Throughout the preparation, quality controls were conducted using the Qiagen Qiaxcel capillary electrophoresis system. Hybridization was performed for 20 h at 48°C.

Quantitative Real-Time PCR

First-strand cDNA from three biological replicates was synthesized from 150 ng DNase-treated total RNA using a mix of oligo(dT)18 and random hexamer primers with the ProtoScript II First Strand cDNA Synthesis Kit (New England Biolabs). Samples were then prepared for the Fluidigm FLEXsix chips according to the manufacturer's manual, and RT-qPCR was performed in technical triplicates on a Fluidigm Biomark HD system. qPCR primers for the target genes were designed using the Primer3 program (Koressaar and Remm, 2007; Untergasser et al., 2012), and sequences can be found in Supplemental Table 1. Data were analyzed using the Fluidigm Real Time PCR Analysis Software v.4.1.2, and relative expression to the control gene serine/threonine-protein phosphatase 2 (Solyc05g006590) was calculated using the $2^{(\Delta Ct)}$ method (Livak and Schmittgen, 2001).

^{13}C-Labeling

For labeling with U^{13}C-glucose: 10 leaves with seven leaflets each were cut from LA1777 plants and immediately put in 50-mL tubes filled with 35 mL U-^{13}C-glucose (99% purity, EUROISO-TOP) (10 g L^{-1} in tap water). The leaves were exposed to permanent light (165 μmol s^{-1} mm^2) for up to 24 h.

For labeling with ^{13}C-CO_2: 6-week-old LA1777 plants grown in hydroponics on expanded clay were placed in a labeling cabinet (PhytolabelBox; developed together with Elektrochemie Halle) (dimensions: 60 × 60 × 60 cm). ^{13}C-CO_2 labeling (99% purity; EUROISO-TOP) in the light (165 μmol s^{-1} mm^2) for up to 180 min was conducted at 380 ppm partial pressure of ^{13}C-CO_2, 70% humidity, and 20% oxygen, which was supplied from synthetic air (Linde). Residual atmospheric CO_2 was removed by flushing the chamber's atmosphere over diver chalk (Spherasorb) for 20 min before the onset of ^{13}C-CO_2-labeling.

For harvest, the leaves were cut at the stalk and were immediately quenched in liquid nitrogen (LN_2). After gentle crushing of leaf matter in a mortar filled with LN_2, leaf pieces and trichomes were separated by shaking for 20 s with crushed dry ice in Schott bottles of 500 mL. During this process, the lid must not be tightly closed to allow pressure release. The frozen leaf pieces and trichome heads obtained were subsequently sieved in liquid nitrogen over 150-μm steel sieves, with the sieve being repeatedly lifted and settled in LN_2. The trichome-free leaf pieces remained on the 150 μm sieve, and the GT heads were collected on a 45-μm sieve. Two biological replicates were made from pools of three plants each (both for leaves and trichomes). All plant matter was lyophilized overnight. Thereafter, these biological replicates were further divided into three aliquots of 25 mg dry weight each, which were extracted and measured independently as technical replicates. The plant material was kept frozen throughout the entire procedure and stored overnight at −25°C to let the dry ice and liquid nitrogen evaporate. Further storage occurred at −80°C. Metabolite extraction was performed as described above. Each pool was extracted in triplicate, resulting in hexuplicate determinations. For LC-MS/MS analysis of the aqueous extraction phase by ion pairing chromatography, a special multiple reaction monitoring method was used where isotopolog isoforms of selected metabolites were recorded using a Sciex 6500 QTRAP and the software Analyst 1.7 (Sciex) (Supplemental Table 4).

Data Analysis

Metabolomics Data

Peak quantification of known compounds by area was done using the software Multiquant 3.0 (Sciex). Retrospective extraction of *m/z* and retention time features from untargeted LC-TOF-MS^1 runs was performed using the software MarkerView 1 (Sciex).

PCA and PLS analysis on dry weight-normalized data was conducted using SIMCA 13.0.3 (Umetrics). For this, each individual metabolite signal of interest was first divided by the average of the corresponding signal in the leaf samples of LA1777. Then, the data ratio was $\log_{10}$ transformed and finally Pareto-scaled. This way, up- and downregulated signals of any intensity are normally distributed but relative changes between trichome and leaf are emphasized. We arbitrarily chose GT of LA1777 to normalize all data.

R2X[1] is the cumulative sum of squares of the entire X that can be explained by principal component 1 (X = log-normalized peak heights relative to LA1777 leaf matter). Q2X(cum) is the cumulative fraction of the total variation of X and Y that can be predicted by principal component 1 for all of its x-variables and y-variables (X = log-normalized peak heights relative to LA1777 leaf matter; Y-variables 1 = GT; 2 = leaves).

Other -Omics Data Processing and Statistical Analysis

Affymetrix exon microarrays were hybridized and imaged using the Affymetrix GeneAtlas System and preprocessed by Affymetrix Power Tools (v. 1.15.1). Multiple probes of each probe set were summarized by median polish. Raw data sets were normalized by robust multiarray averaging. To remove background noise, data were filtered for undetected probe

sets as described by Lockstone (2011) using detection above background tests at the exon-level implemented in APT. Undetected probe sets were excluded prior to differential gene expression analysis.

Linear models were fitted with Bioconductor's limma package (Smyth, 2005) and P values were adjusted using Benjamini and Hochberg FDR (<0.05) procedure (Benjamini and Hochberg, 1995). Differentially expressed genes were identified by a significance threshold of 0.05 and a minimal $\log_2$-fold change of ± 1.

Low expressed proteins detected by quantitative shotgun proteomics were filtered by an independent filtering approach using the genefilter package (Gentleman, 2009) and excluded from further analyses. The PLGEM package (Pavelka et al., 2004) was used for differential expression analyses with a significance threshold of 0.01. The suitability of this package for analyzing data sets derived from shotgun proteomics was proven earlier (Pavelka et al., 2008).

After data processing and normalization, 20,445 genes and 4390 proteins annotated with a Solyc tomato ID formed the basis for gene expression and protein abundance analysis between trichomes and trichome-free leaves. Individual values as well as the averages of triplicates, $\log_2$-fold change between groups and the FDR-adjusted P values from a moderated *t* test (Smyth, 2005) are shown in Supplemental Data Set 5. Principal component analysis and hierarchical clustering demonstrating that replicates group together as expected are shown in Supplemental Figure 17.

Correlation between transcriptomics and proteomics within tissues was estimated by calculating the Pearson coefficient, which produced slightly positive *r* values of 0.341 (LA1777 leaf), 0.367 (LA1777 trichome), 0.418 (LA4024 leaf), and 0.414 (LA4024 trichome). Moderately positive correlations between transcriptome and proteome data are usual and have been reported previously (Maier et al., 2009). In a recent study in maize (*Zea mays*), similar correlations values were observed, but enrichment categories were found to be highly similar between transcriptome and proteome data (Walley et al., 2016). The enrichment analysis (see Supplemental Data Set 6) points to a similar trend. Functional categories that show a strong enrichment at the transcriptome level are also enriched at the proteome level (e.g., photosynthesis, Calvin cycle, isoprenoid metabolism, and lipid metabolism).

The MapMan hierarchical ontology was used for functional annotation of the studied transcriptomes and proteomes of both *Solanum* species (Thimm et al., 2004). The official mapping file for the ITAG 2.3 release was used in all subsequent analyses. Enrichment analyses were performed using PageMan in the MapMan program.

Phylogenetic Analysis

A phylogenetic tree of the BASS protein family from *Arabidopsis thaliana* and tomato (*S. lycopersicum*) was generated with the Geneious software v 6.1.8 (www.geneious.com). First the BASS protein sequences from these two species were aligned using the MUSCLE alignment algorithm with the following options: maximum number of iterations = 10; distance measure = kmer6_6 for the first two iterations then pctid_kimura for the subsequent ones, clustering method = UPGMB; tree rooting method = pseudo; sequence weighing scheme = ClustalW; terminal gaps = half penalty; objective score = spm; anchor spacing = 32; gap open score = −1. The alignment was then fed into the Geneious Tree Builder with the following options: genetic distance model = Jukes-Cantor; tree build method = neighbor-joining without outgroup; number of replicates for the bootstrap resampling = 1000; support threshold of 45%. The tree was then exported in the unrooted layout to Corel Draw for manual editing and annotating of BASS functions.

Prediction of the Subcellular Localization

The protein sequence of the individual SolGene ID was loaded into Wolf PSort (accessible via http://www.genscript.com/wolf-psort.html), Sherloc2 (http://abi.inf.uni-tuebingen.de/Services/SherLoc2), and iPSort (http://ipsort.hgc.jp). In some cases, the respective protein sequences were blasted against the closest homolog in Arabidopsis and the SUBA prediction tool was also used (accessible via http://www.arabidopsis.org).

Light Microscopy

Microscopy analysis of leaves and trichomes was performed as previously published (Bergau et al., 2015). Trichomes on the leaves were observed in bright field with an AZ100 (Nikon). Fluorescence was observed with a LSM 710 microscope (Zeiss). Autofluorescence was excited at 405 nm and recorded at 420 to 545 nm (cell wall) and 645 to 735 nm (chloroplasts).

Transmission Electron Microscopy

Leaves and trichomes were fixed with 3% glutaraldehyde (Sigma-Aldrich) in sodium cacodylate buffer (SCB), pH 7.2, for 4 h at room temperature, washed with SCB, postfixed with 1% osmium tetroxide (Carl Roth) in SCB, dehydrated in a graded ethanol series, and embedded in epoxy resin. After polymerization, the material was sectioned with an Ultramicrotome S (Leica). Ultrathin sections (80 nm) were transferred to formvar-coated grids and poststained with uranyl acetate and lead citrate. The sections were observed with a Zeiss Libra 120 transmission electron microscope operating at 120 kV (Carl Zeiss Microscopy). Images were taken applying a Dual-Speed on axis SSCCD camera (BM-2k-120; TRS).

ROS Staining

Staining with dihydroethidium (Sigma-Aldrich) was performed according to Owusu-Ansah et al. (2008). Instead of the described buffer, a sorbitol buffer (200 mM sorbitol, 50 mM Tris-Cl, 20 mM Suc, 10 mM KCl, 5 mM $MgCl_2$, 5 mM succinic acid, 1 mM EGTA, 0.5 mM K_2HPO_4, and 0.015% Triton X-100) was used. Staining occurred after 3×3 min vacuum filtration of a single tomato leaflet. The laser emission wavelength was 514 nm. The fluorescence readout window was set to 540 to 620 nm.

Accession Numbers

The metabolomics raw data and metabolite abundances are available at MetaboLights under the accession number MTBLS297. The mass spectrometry proteomics data have been deposited to the ProteomeXchange Consortium via the PRIDE partner repository with the data set identifier PXD003154. Transcriptomics raw data are available in ArrayExpress under the accession number E-MTAB-4482.

Supplemental Data

Supplemental Figure 1. Venn diagrams of differentially regulated -omics signals with a $\log_2$-fold change >1.

Supplemental Figure 2. Total GC-MS and LC-MS ion chromatograms from *S. habrochaites* LA1777 and *S. lycopersicum* LA4024 extracts.

Supplemental Figure 3. Fatty acid and oxylipin peak areas from trichome and trichome-free leaf extracts.

Supplemental Figure 4. MS/MS spectra of a peak eluting at 13.8 min with [M-H]: *m/z* 295.228.

Supplemental Figure 5. Scores of a principle component analysis comparing 115 selected signals from hydrophilic extracts of leaves (LVS) and trichomes (TRI) of LA1777 and LA4024.

Supplemental Figure 6. MapMan transcriptomics and proteomics overview of the cellular metabolism in LA4024.

Supplemental Figure 7. MapMan proteomics overview of the cellular metabolism in LA1777.

Supplemental Figure 8. Time course after pulse labeling of LA1777 with ^{13}C-CO_2 and U-^{13}C-D-glucose.

Supplemental Figure 9. Biosynthesis of isoprenoid precursors in leaves and trichomes of LA4024 and LA1777.

Supplemental Figure 10. ROS staining of LA1777 using dihydroethidium and laser scanning microscopy.

Supplemental Figure 11. Transcript levels and protein abundances of lipoxygenases of cytosolic and plastidic localization.

Supplemental Figure 12. Differential transcript and protein levels of REDOX enzyme families.

Supplemental Figure 13. ^{13}C-incorporation into citrate and isocitrate after 24 h labeling of LA1777 with U-^{13}C-D-glucose in permanent light.

Supplemental Figure 14. MapMan overview of cytosolic and plastidic glycolysis and plastid transporters (triose phosphate, putative pyruvate, and malate) in LA1777.

Supplemental Figure 15. Phylogenetic tree of proteins of the bile acid sodium symporter family from *Arabidopsis thaliana* and *Solanum lycopersicum*.

Supplemental Figure 16. Expression of NADPH-producing enzyme families in GT versus trichome-free leaves.

Supplemental Figure 17. Principle component and hierarchical cluster analyses of transcriptome and proteome data.

Supplemental Table 1. Genes whose expression was verified by qRT-PCR and corresponding primers.

Supplemental Table 2. List of genes of the MEV and MEP pathways.

Supplemental Table 3. Chromatography conditions.

Supplemental Table 4. MS parameters for the untargeted analysis of hydrophilic and semipolar metabolites by (−)ESI-SWATH-MS/MS.

Supplemental Table 5. Summary of RNA-seq samples and data.

Supplemental Data Set 1. Peak heights of semipolar metabolites as extracted from TOF-MS1 by MarkerView (ESI negative).

Supplemental Data Set 2. Peak heights of hydrophilic metabolites as extracted from TOF-MS1 by MarkerView (ESI negative).

Supplemental Data Set 3. Peak areas of hydrophilic metabolites.

Supplemental Data Set 4. Prediction of loadings of the principal component analysis of hydrophilic metabolites.

Supplemental Data Set 5. Transcriptomics and proteomics data.

Supplemental Data Set 6. Enrichment analysis.

Supplemental Data Set 7. SD (n = 6 measurements) of isotopologs from 13C-labeling experiments.

Supplemental Data Set 8. Multiple alignment of BASS proteins from *Arabidopsis thaliana* and *Solanum lycopersicum*.

Supplemental Data Set 9. MS parameters for the targeted analysis of selected metabolites and their ^{13}C-isotopologs via (−)ESI and scheduled multiple reaction monitoring.

ACKNOWLEDGMENTS

We thank Gerd Hause for assistance with electron microscopy (Biozentrum, Martin-Luther Universität Halle-Wittenberg) and Mario Bauer at the Helmholtz-Centre for Environmental Research for providing access to the Biomark HD system. We thank Michael Hahn and coworkers of Elektrochemie Halle for the collaborative development of a prototype for ^{13}C-phytolabeling. This work was funded in part by the Deutsche Forschungsgemeinschaft (Grant TI 800/1) to A.T.

AUTHOR CONTRIBUTIONS

G.U.B. developed the metabolite profiling approach and the PhytolabelBox in collaboration with Elektrochemie Halle, performed the -omics data analysis, and wrote the manuscript. S.B. extracted RNA, conducted hybridizations, and performed RT-qPCR and GC-MS runs. N.B. prepared the plant material and extracts, conducted LC-MS runs, contributed to the data analysis, performed ROS staining, and generated micrographs. A.H. assisted G.U.B. and N.B. with sample preparation. B.A. performed bioinformatics data analysis of transcriptome and proteome data. P.M. and W.H. performed shotgun proteomics measurements and analysis. J.M.J.-G. analyzed the RNA-seq data of tomato and designed the gene expression microarray based on these data. A.T. conceived and supervised the project, performed transcriptome and proteome data analysis, and wrote the manuscript. All authors read and revised the manuscript.

Received January 24, 2017; revised March 24, 2017; accepted April 12, 2017; published April 13, 2017.

REFERENCES

Balcke, G.U., Bennewitz, S., Zabel, S., and Tissier, A. (2014). Isoprenoid and metabolite profiling of plant trichomes. Methods Mol. Biol. **1153:** 189–202.

Benjamini, Y., and Hochberg, Y. (1995). Controlling the false discovery rate - a practical and powerful approach to multiple testing. J. R. Stat. Soc. B Met. **57:** 289–300.

Bergau, N., Bennewitz, S., Syrowatka, F., Hause, G., and Tissier, A. (2015). The development of type VI glandular trichomes in the cultivated tomato *Solanum lycopersicum* and a related wild species *S. habrochaites*. BMC Plant Biol. **15:** 289.

Besser, K., Harper, A., Welsby, N., Schauvinhold, I., Slocombe, S., Li, Y., Dixon, R.A., and Broun, P. (2009). Divergent regulation of terpenoid metabolism in the trichomes of wild and cultivated tomato species. Plant Physiol. **149:** 499–514.

Bleeker, P.M., Mirabella, R., Diergaarde, P.J., VanDoorn, A., Tissier, A., Kant, M.R., Prins, M., de Vos, M., Haring, M.A., and Schuurink, R.C. (2012). Improved herbivore resistance in cultivated tomato with the sesquiterpene biosynthetic pathway from a wild relative. Proc. Natl. Acad. Sci. USA **109:** 20124–20129.

Bleeker, P.M., Diergaarde, P.J., Ament, K., Schütz, S., Johne, B., Dijkink, J., Hiemstra, H., de Gelder, R., de Both, M.T., Sabelis, M.W., Haring, M.A., and Schuurink, R.C. (2011). Tomato-produced 7-epizingiberene and R-curcumene act as repellents to whiteflies. Phytochemistry **72:** 68–73.

Brückner, K., Božić, D., Manzano, D., Papaefthimiou, D., Pateraki, I., Scheler, U., Ferrer, A., de Vos, R.C., Kanellis, A.K., and Tissier, A. (2014). Characterization of two genes for the biosynthesis of abietane-type diterpenes in rosemary (*Rosmarinus officinalis*) glandular trichomes. Phytochemistry **101:** 52–64.

Caspi, R., et al. (2014). The MetaCyc database of metabolic pathways and enzymes and the BioCyc collection of Pathway/Genome Databases. Nucleic Acids Res. **42:** D459–D471.

Chen, Z.H., Walker, R.P., Acheson, R.M., and Leegood, R.C. (2002). Phosphoenolpyruvate carboxykinase assayed at physiological concentrations of metal ions has a high affinity for CO_2. Plant Physiol. **128:** 160–164.

Coates, R.M., Denissen, J.F., Juvik, J.A., and Babka, B.A. (1988). Identification of alpha-santalenoic and endo-beta-bergamotenoic acids as moth oviposition stimulants from wild tomato leaves. J. Org. Chem. **53:** 2186–2192.

Croteau, R.B., Davis, E.M., Ringer, K.L., and Wildung, M.R. (2005). (-)-Menthol biosynthesis and molecular genetics. Naturwissenschaften **92:** 562–577.

Cui, H., Zhang, S.T., Yang, H.J., Ji, H., and Wang, X.J. (2011). Gene expression profile analysis of tobacco leaf trichomes. BMC Plant Biol. **11:** 76.

Dudareva, N., Andersson, S., Orlova, I., Gatto, N., Reichelt, M., Rhodes, D., Boland, W., and Gershenzon, J. (2005). The nonmevalonate pathway supports both monoterpene and sesquiterpene formation in snapdragon flowers. Proc. Natl. Acad. Sci. USA **102:** 933–938.

Eisenhut, M., Hocken, N., and Weber, A.P.M. (2015). Plastidial metabolite transporters integrate photorespiration with carbon, nitrogen, and sulfur metabolism. Cell Calcium **58:** 98–104.

Ekanayaka, E.A.P., Li, C., and Jones, A.D. (2014). Sesquiterpenoid glycosides from glandular trichomes of the wild tomato relative *Solanum habrochaites*. Phytochemistry **98:** 223–231.

Fahn, A. (2000). Structure and function of secretory cells. In Plant Trichomes, D.L. Hallahan and J.C. Gray, eds (New York: Academic Press), pp. 37–75.

Flügge, U.I., Häusler, R.E., Ludewig, F., and Gierth, M. (2011). The role of transporters in supplying energy to plant plastids. J. Exp. Bot. **62:** 2381–2392.

Fobes, J.F., Mudd, J.B., and Marsden, M.P. (1985). Epicuticular lipid accumulation on the leaves of *Lycopersicon pennellii* (Corr.) D'Arcy and *Lycopersicon esculentum* Mill. Plant Physiol. **77:** 567–570.

Frelichowski, J.E., and Juvik, J.A. (2005). Inheritance of sesquiterpene carboxylic acid synthesis in crosses of *Lycopersicon hirsutum* with insect-susceptible tomatoes. Plant Breed. **124:** 277–281.

Furumoto, T., et al. (2011). A plastidial sodium-dependent pyruvate transporter. Nature **476:** 472–475.

Gang, D.R., Wang, J., Dudareva, N., Nam, K.H., Simon, J.E., Lewinsohn, E., and Pichersky, E. (2001). An investigation of the storage and biosynthesis of phenylpropenes in sweet basil. Plant Physiol. **125:** 539–555.

Gentleman, R., Carey, V., Huber, W., and Hahne, F. (2009). Genefilter: methods for filtering gens from microarray experiments. R Package Version 1.24.2, http://bioconductor.org/packages/release/bioc/html/genefilter.html.

Ghosh, B., Westbrook, T.C., and Jones, A.D. (2014). Comparative structural profiling of trichome specialized metabolites in tomato (*Solanum lycopersicum*) and *S. habrochaites*: acylsugar profiles revealed by UHPLC/MS and NMR. Metabolomics **10:** 496–507.

Gigolashvili, T., Yatusevich, R., Rollwitz, I., Humphry, M., Gershenzon, J., and Flügge, U.I. (2009). The plastidic bile acid transporter 5 is required for the biosynthesis of methionine-derived glucosinolates in *Arabidopsis thaliana*. Plant Cell **21:** 1813–1829.

Glas, J.J., Schimmel, B.C.J., Alba, J.M., Escobar-Bravo, R., Schuurink, R.C., and Kant, M.R. (2012). Plant glandular trichomes as targets for breeding or engineering of resistance to herbivores. Int. J. Mol. Sci. **13:** 17077–17103.

Hopfgartner, G., Tonoli, D., and Varesio, E. (2012). High-resolution mass spectrometry for integrated qualitative and quantitative analysis of pharmaceuticals in biological matrices. Anal. Bioanal. Chem. **402:** 2587–2596.

Jin, J., Panicker, D., Wang, Q., Kim, M.J., Liu, J., Yin, J.L., Wong, L., Jang, I.C., Chua, N.H., and Sarojam, R. (2014). Next generation sequencing unravels the biosynthetic ability of spearmint (*Mentha spicata*) peltate glandular trichomes through comparative transcriptomics. BMC Plant Biol. **14:** 292.

Kim, J., Kang, K., Gonzales-Vigil, E., Shi, F., Jones, A.D., Barry, C.S., and Last, R.L. (2012). Striking natural diversity in glandular trichome acylsugar composition is shaped by variation at the Acyltransferase2 locus in the wild tomato *Solanum habrochaites*. Plant Physiol. **160:** 1854–1870.

Kim, J., Matsuba, Y., Ning, J., Schilmiller, A.L., Hammar, D., Jones, A.D., Pichersky, E., and Last, R.L. (2014). Analysis of natural and induced variation in tomato glandular trichome flavonoids identifies a gene not present in the reference genome. Plant Cell **26:** 3272–3285.

Kokwaro, G. (2009). Ongoing challenges in the management of malaria. Malar. J. **8** (suppl. 1): S2.

Koressaar, T., and Remm, M. (2007). Enhancements and modifications of primer design program Primer3. Bioinformatics **23:** 1289–1291.

Kunst, L., and Samuels, L. (2009). Plant cuticles shine: advances in wax biosynthesis and export. Curr. Opin. Plant Biol. **12:** 721–727.

Li, C., Wang, Z., and Jones, A.D. (2014). Chemical imaging of trichome specialized metabolites using contact printing and laser desorption/ionization mass spectrometry. Anal. Bioanal. Chem. **406:** 171–182.

Lipko, A., and Swiezewska, E. (2016). Isoprenoid generating systems in plants - A handy toolbox how to assess contribution of the mevalonate and methylerythritol phosphate pathways to the biosynthetic process. Prog. Lipid Res. **63:** 70–92.

Livak, K.J., and Schmittgen, T.D. (2001). Analysis of relative gene expression data using real-time quantitative PCR and the 2(-Delta Delta C(T)) method. Methods **25:** 402–408.

Lockstone, H.E. (2011). Exon array data analysis using Affymetrix power tools and R statistical software. Brief. Bioinform. **12:** 634–644.

Ludewig, F., and Flügge, U.-I. (2013). Role of metabolite transporters in source-sink carbon allocation. Front. Plant Sci. **4:** 231.

Maier, T., Güell, M., and Serrano, L. (2009). Correlation of mRNA and protein in complex biological samples. FEBS Lett. **583:** 3966–3973.

McDowell, E.T., et al. (2011). Comparative functional genomic analysis of *Solanum glandular* trichome types. Plant Physiol. **155:** 524–539.

Nonomura, T., Xu, L., Wada, M., Kawamura, S., Miyajima, T., Nishitomi, A., Kakutani, K., Takikawa, Y., Matsuda, Y., and Toyoda, H. (2009). Trichome exudates of *Lycopersicon pennellii* form a chemical barrier to suppress leaf-surface germination of *Oidium neolycopersici* conidia. Plant Sci. **176:** 31–37.

Oliver, D.J., Nikolau, B.J., and Wurtele, E.S. (2009). Acetyl-CoA-Life at the metabolic nexus. Plant Sci. **176:** 597–601.

Owusu-Ansah, E., Yavari, A., and Banerjee, U. (2008). A protocol for in vivo detection of reactive oxygen species. Protoc. Exch., http://dx.doi.org/10.1038/nprot.2008.23.

Pavelka, N., Pelizzola, M., Vizzardelli, C., Capozzoli, M., Splendiani, A., Granucci, F., and Ricciardi-Castagnoli, P. (2004). A power law global error model for the identification of differentially expressed genes in microarray data. BMC Bioinformatics **5:** 203.

Pavelka, N., Fournier, M.L., Swanson, S.K., Pelizzola, M., Ricciardi-Castagnoli, P., Florens, L., and Washburn, M.P. (2008). Statistical similarities between transcriptomics and quantitative shotgun proteomics data. Mol. Cell. Proteomics **7:** 631–644.

Sallaud, C., Rontein, D., Onillon, S., Jabès, F., Duffé, P., Giacalone, C., Thoraval, S., Escoffier, C., Herbette, G., Leonhardt, N., Causse, M., and Tissier, A. (2009). A novel pathway for sesquiterpene biosynthesis from Z,Z-farnesyl pyrophosphate in the wild tomato *Solanum habrochaites*. Plant Cell **21:** 301–317.

Samuels, L., Kunst, L., and Jetter, R. (2008). Sealing plant surfaces: cuticular wax formation by epidermal cells. Annu. Rev. Plant Biol. **59:** 683–707.

Savchenko, T., Walley, J.W., Chehab, E.W., Xiao, Y., Kaspi, R., Pye, M.F., Mohamed, M.E., Lazarus, C.M., Bostock, R.M., and Dehesh, K. (2010). Arachidonic acid: an evolutionarily conserved signaling molecule modulates plant stress signaling networks. Plant Cell **22:** 3193–3205.

Schilmiller, A., Shi, F., Kim, J., Charbonneau, A.L., Holmes, D., Daniel Jones, A., and Last, R.L. (2010). Mass spectrometry screening reveals widespread diversity in trichome specialized

metabolites of tomato chromosomal substitution lines. Plant J. **62:** 391–403.

Schilmiller, A.L., Charbonneau, A.L., and Last, R.L. (2012). Identification of a BAHD acetyltransferase that produces protective acyl sugars in tomato trichomes. Proc. Natl. Acad. Sci. USA **109:** 16377–16382.

Schilmiller, A.L., Schauvinhold, I., Larson, M., Xu, R., Charbonneau, A.L., Schmidt, A., Wilkerson, C., Last, R.L., and Pichersky, E. (2009). Monoterpenes in the glandular trichomes of tomato are synthesized from a neryl diphosphate precursor rather than geranyl diphosphate. Proc. Natl. Acad. Sci. USA **106:** 10865–10870.

Schmid-Siegert, E., Stepushenko, O., Glauser, G., and Farmer, E.E. (2016). Membranes as structural antioxidants: Recycling of malondialdehyde to its source in oxidation-sensitive chloroplast fatty acids. J. Biol. Chem. **291:** 13005–13013.

Schmidt, A., Li, C., Shi, F., Jones, A.D., and Pichersky, E. (2011). Polymethylated myricetin in trichomes of the wild tomato species *Solanum habrochaites* and characterization of trichome-specific 3′/5′- and 7/4′-myricetin O-methyltransferases. Plant Physiol. **155:** 1999–2009.

Schwender, J., Goffman, F., Ohlrogge, J.B., and Shachar-Hill, Y. (2004). Rubisco without the Calvin cycle improves the carbon efficiency of developing green seeds. Nature **432:** 779–782.

Shtaida, N., Khozin-Goldberg, I., and Boussiba, S. (2015). The role of pyruvate hub enzymes in supplying carbon precursors for fatty acid synthesis in photosynthetic microalgae. Photosynth. Res. **125:** 407–422.

Slocombe, S.P., Schauvinhold, I., McQuinn, R.P., Besser, K., Welsby, N.A., Harper, A., Aziz, N., Li, Y., Larson, T.R., Giovannoni, J., Dixon, R.A., and Broun, P. (2008). Transcriptomic and reverse genetic analyses of branched-chain fatty acid and acyl sugar production in Solanum pennellii and *Nicotiana benthamiana*. Plant Physiol. **148:** 1830–1846.

Smyth, G.K. (2005). Limma: linear models for microarray data. In Bioinformatics and Computational Biology Solutions Using {R} and Bioconductor, V. Gentleman, S. Dudoit, R. Irizarry, and W. Huber, eds (New York: Springer), pp. 397–420.

Soetaert, S.S., Van Neste, C.M., Vandewoestyne, M.L., Head, S.R., Goossens, A., Van Nieuwerburgh, F.C., and Deforce, D.L. (2013). Differential transcriptome analysis of glandular and filamentous trichomes in *Artemisia annua*. BMC Plant Biol. **13:** 220.

Tomato Genome Consortium (2012). The tomato genome sequence provides insights into fleshy fruit evolution. Nature **485:** 635–641.

Tcherkez, G., Mahé, A., Boex-Fontvieille, E., Gout, E., Guérard, F., and Bligny, R. (2011). Experimental evidence of phosphoenolpyruvate resynthesis from pyruvate in illuminated leaves. Plant Physiol. **157:** 86–95.

Thimm, O., Bläsing, O., Gibon, Y., Nagel, A., Meyer, S., Krüger, P., Selbig, J., Müller, L.A., Rhee, S.Y., and Stitt, M. (2004). MAPMAN: a user-driven tool to display genomics data sets onto diagrams of metabolic pathways and other biological processes. Plant J. **37:** 914–939.

Tissier, A. (2012). Glandular trichomes: what comes after expressed sequence tags? Plant J. **70:** 51–68.

Turner, G.W., Gershenzon, J., and Croteau, R.B. (2000). Development of peltate glandular trichomes of peppermint. Plant Physiol. **124:** 665–680.

Untergasser, A., Cutcutache, I., Koressaar, T., Ye, J., Faircloth, B.C., Remm, M., and Rozen, S.G. (2012). Primer3–new capabilities and interfaces. Nucleic Acids Res. **40:** e115.

van Der Hoeven, R.S., Monforte, A.J., Breeden, D., Tanksley, S.D., and Steffens, J.C. (2000). Genetic control and evolution of sesquiterpene biosynthesis in *Lycopersicon esculentum* and *L. hirsutum*. Plant Cell **12:** 2283–2294.

Walley, J.W., Sartor, R.C., Shen, Z., Schmitz, R.J., Wu, K.J., Urich, M.A., Nery, J.R., Smith, L.G., Schnable, J.C., Ecker, J.R., and Briggs, S.P. (2016). Integration of omic networks in a developmental atlas of maize. Science **353:** 814–818.

Weber, A.P.M., and Bräutigam, A. (2013). The role of membrane transport in metabolic engineering of plant primary metabolism. Curr. Opin. Biotechnol. **24:** 256–262.

Xiao, Y., Savchenko, T., Baidoo, E.E.K., Chehab, W.E., Hayden, D.M., Tolstikov, V., Corwin, J.A., Kliebenstein, D.J., Keasling, J.D., and Dehesh, K. (2012). Retrograde signaling by the plastidial metabolite MEcPP regulates expression of nuclear stress-response genes. Cell **149:** 1525–1535.

Xing, S., van Deenen, N., Magliano, P., Frahm, L., Forestier, E., Nawrath, C., Schaller, H., Gronover, C.S., Prüfer, D., and Poirier, Y. (2014). ATP citrate lyase activity is post-translationally regulated by sink strength and impacts the wax, cutin and rubber biosynthetic pathways. Plant J. **79:** 270–284.